Perceiving the Emergence of Hadron Mass through **AMBER@CERN**

27 April to 30 April 2021
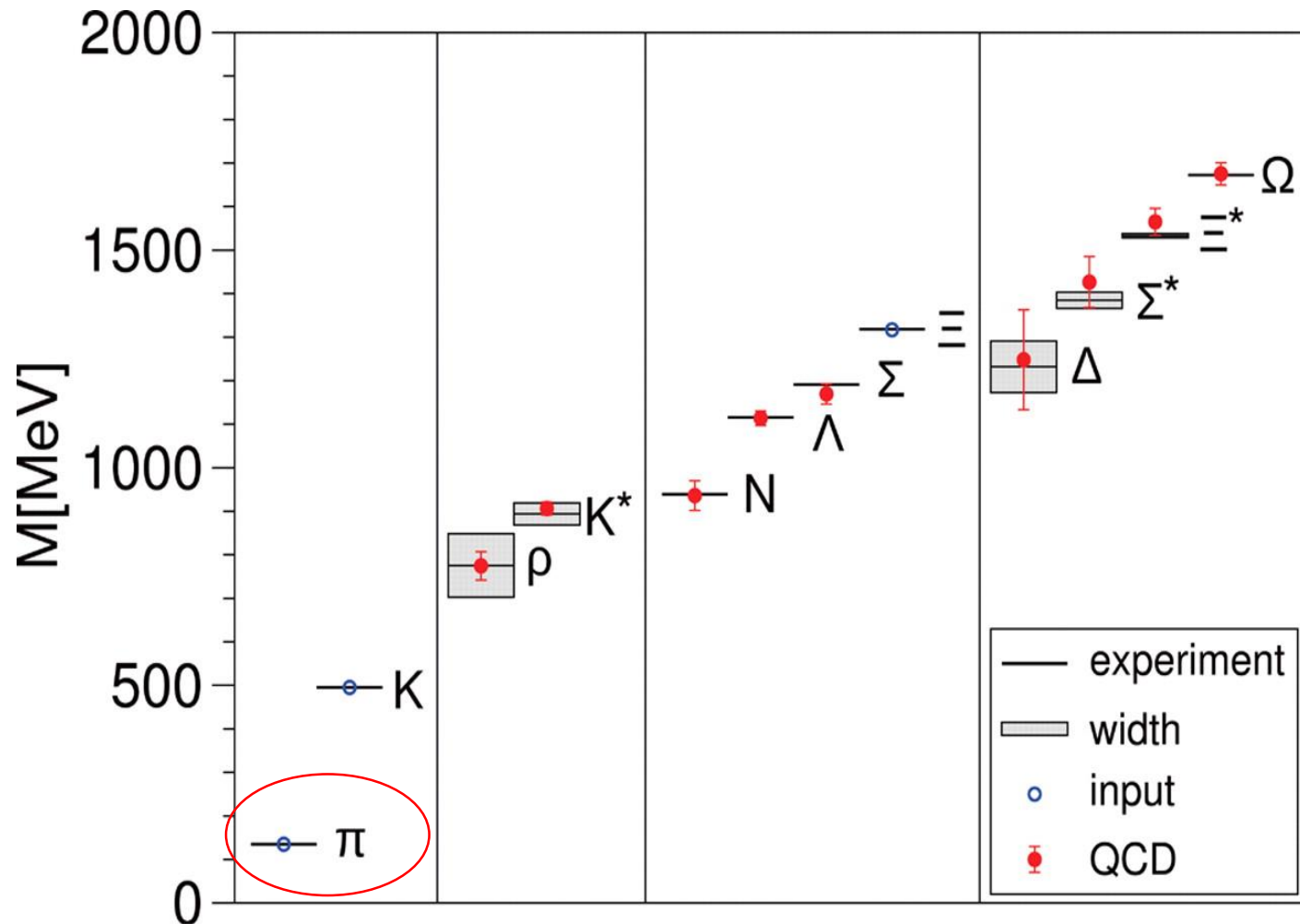CERN, Geneve - Switzerland

Accessing pion's large-x gluon by fixed-target charmonium production

Wen-Chen Chang

Institute of Physics, Academia Sinica, Taiwan

In collaboration with
Chia-Yu Hsieh, Yu-Shiang Lian,
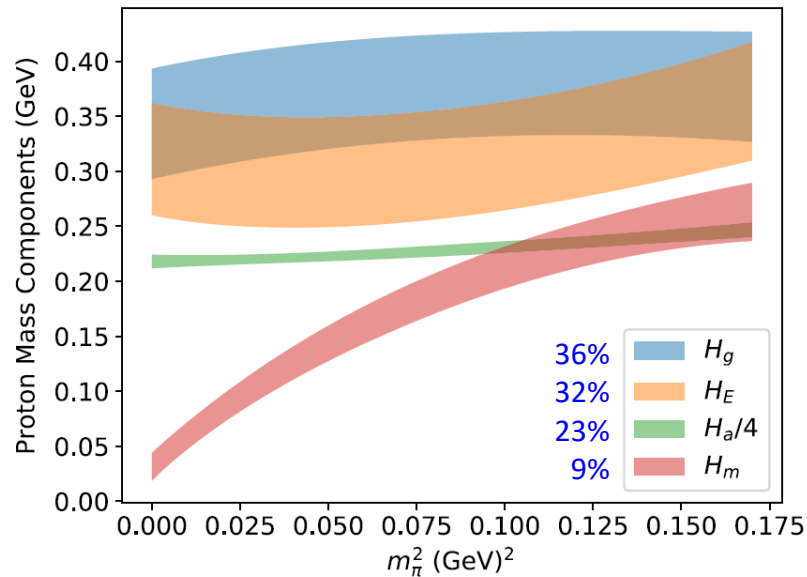*Jen-Chieh Peng, Stephane Platchkov, and Takahiro Sawada*

Light hadron spectrum

Mass Decomposition of Proton and Pion from Lattice

Proton

PRL 121, 212001 (2018)

Pion

PRD 91, 074516 (2015)

$$M = -\langle T_{44} \rangle = \langle H_m \rangle + \langle H_E \rangle (\mu) + \langle H_g \rangle (\mu) + \frac{1}{4} \langle H_a \rangle$$

Quark energy   Trace Anomaly

Quark mass   Gluon energy
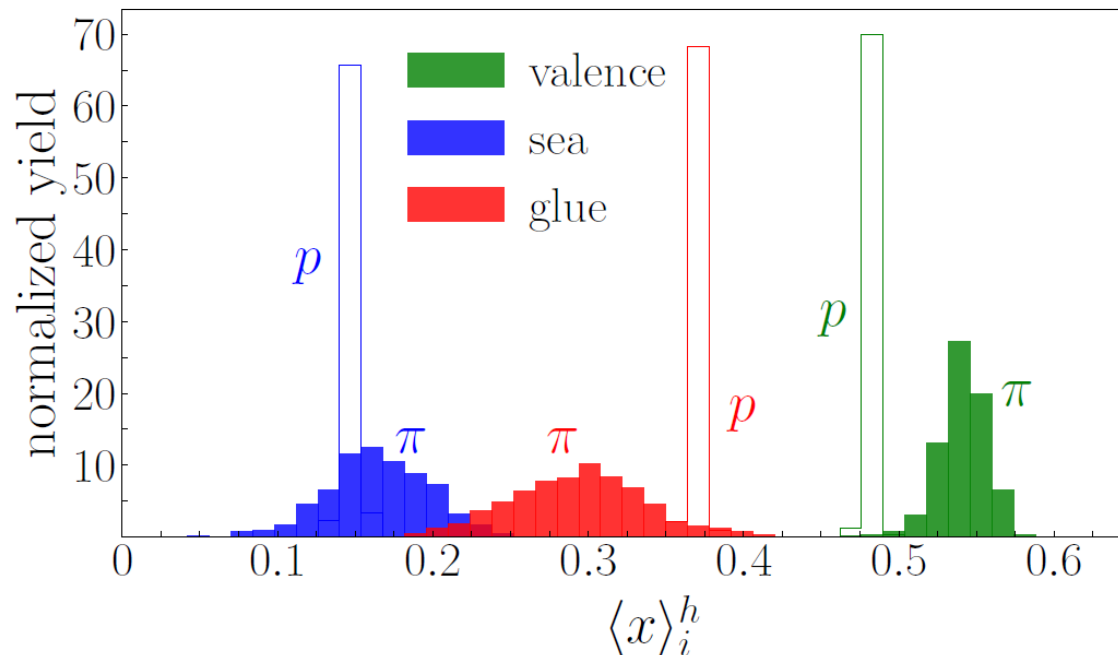
3
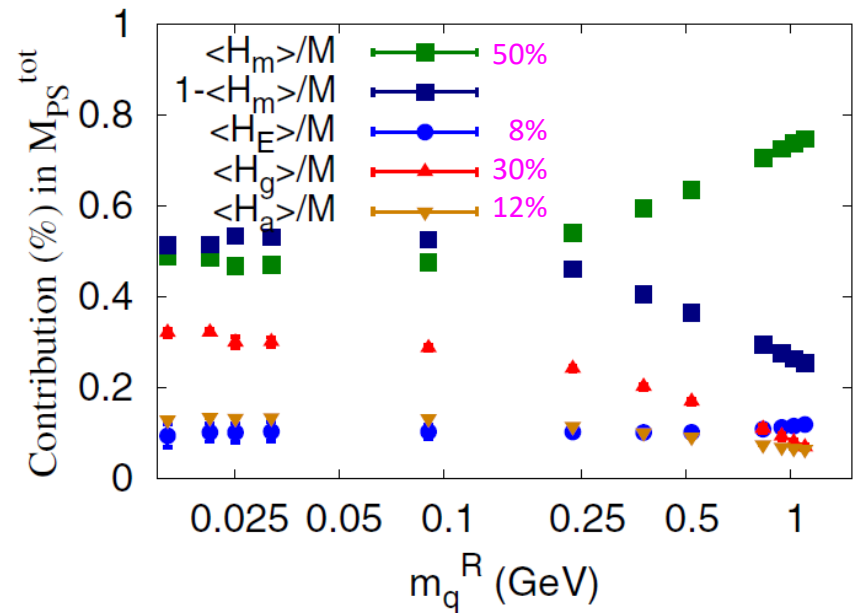
JAM21, arXiv:2103.02159

FIG. 14. Normalized yield of momentum fractions $\langle x \rangle_i^h$ of the proton ($h = p$, open) and pion ($h = \pi$, shaded), evaluated at the input scale, $\mu^2 = m_c^2$, for valence quarks (green), sea quarks (blue), and gluons (red). The proton PDFs used in calculating $\langle x \rangle_i^p$ are taken from Ref. [24].

Experimental Approaches of Accessing Pion Structure

- Drell-Yan: $\pi^{\pm} p \to \mu^+ \mu^- X$ (LO: sensitive to valence quarks)
  - **LO: $q\bar{q} \to \mu^+ \mu^-$**
  - NLO: $q\bar{q} \to \mu^+ \mu^- G, qG \to \mu^+ \mu^- q$ (large p_T)
  - NNLO: $q\bar{q}G \to \mu^+ \mu^- G, qG \to \mu^+ \mu^- qG, GG \to \mu^+ \mu^- q\bar{q}$
- Direct photon: $\pi^{\pm} p \to \gamma X$ (LO: sensitive to gluons)
  - **LO: $q\bar{q} \to \gamma G, qG \to \gamma q$**
- Jpsi: $\pi^{\pm} p \to J/\psi X$ (LO: sensitive to gluons)
  - **LO: $q\bar{q} \to c\bar{c} \to J/\psi X, GG \to c\bar{c} \to J/\psi X$**
  - NLO: $q\bar{q} \to c\bar{c}G \to J/\psi X, GG \to c\bar{c}G \to J/\psi X, qG \to c\bar{c}q \to J/\psi X$
- Leading neutron (LN) electroproduction: Sullivan processes from a nucleon's pion cloud

5
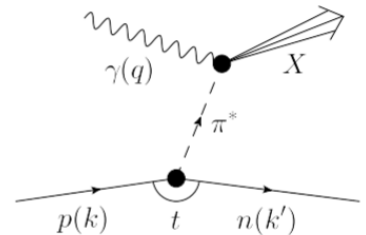
Pion PDFs (2021)

PDF	DY (xF, pT)	Direct γ	J/ψ	LN	Refs.
OW	*		*		PRD 1984
ABFKW	*	*			PLB 1989
SMRS	*	*			PRD 1992
GRV	*	*			ZPC 1992
GRS	*				EPJC 1999
JAM18	*			*	PRL 2018
BS	*				NPA 2019 PLB 2021
xFitter	*	*			PRD 2020
JAM21	*			*	2103.02159

Pion PDFs

$$Q^2 = 9.6 \text{ GeV}^2$$
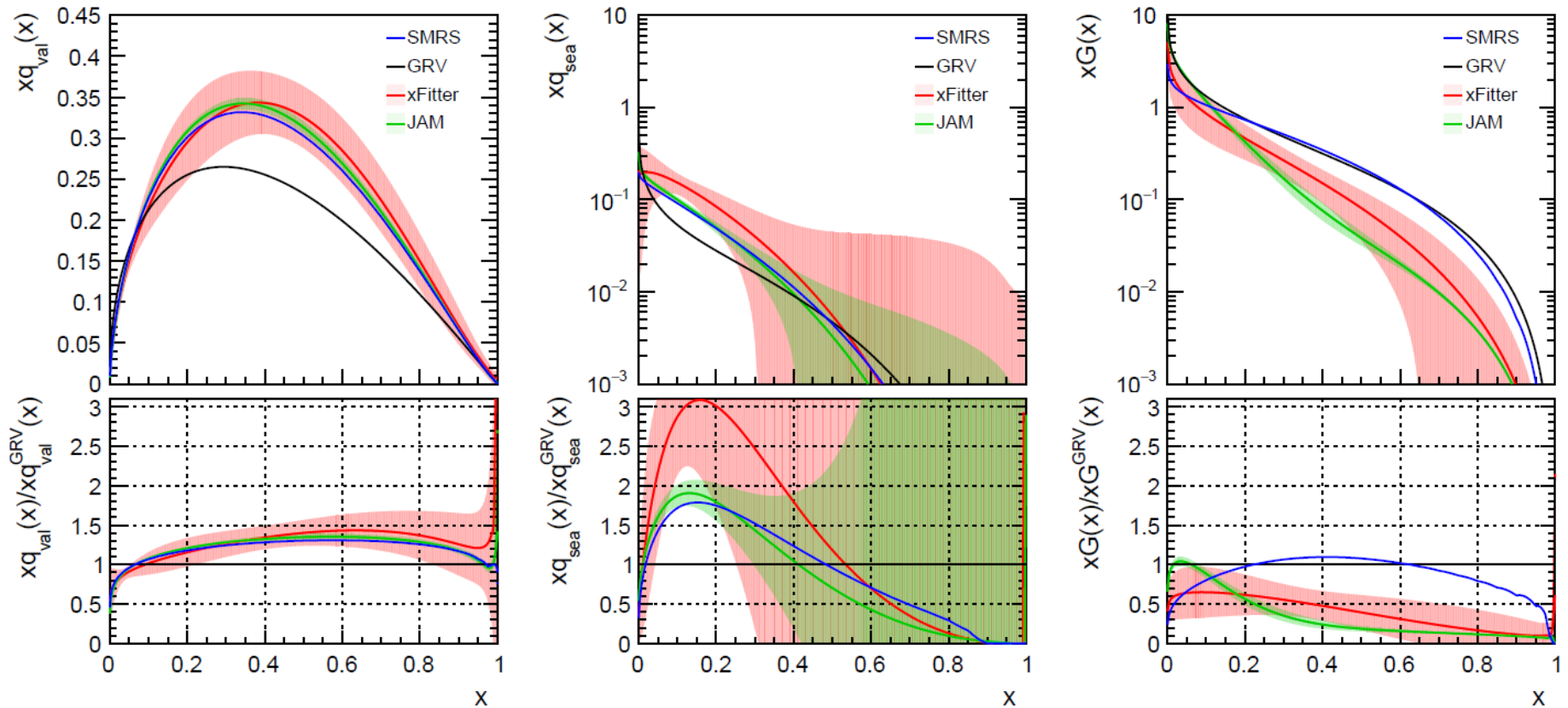
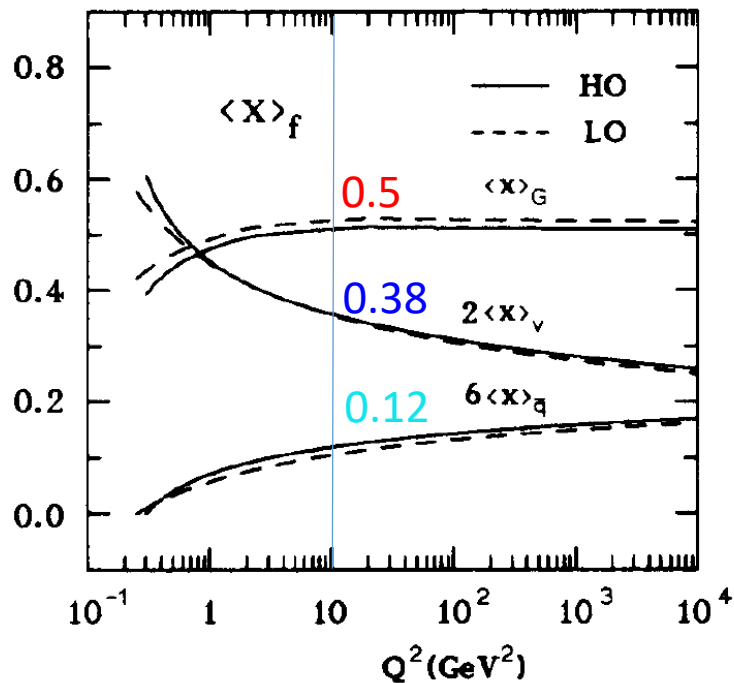Large discrepancy of valence quark and gluon densities at x>0.1 is seen

GRV vs. JAM

GRV

JAM

data sets	$\langle x \rangle_v^\pi$	$\langle x \rangle_s^\pi$	$\langle x \rangle_g^\pi$
		$\mu^2 = 10\ \mathrm{GeV}^2$	
DY	0.49(1)	0.26(8)	0.25(8)
DY+LN	0.43(2)	0.17(3)	0.40(4)
DY+LN+DYp_{T}	**0.44(1)**	**0.19(2)**	**0.37(3)**

The hierarchy of <x> of valence quark and gluon are opposite in GRV and JAM.

Pion-induced J/psi Production - Fixed-target Experiments

Paper	Reference	Year	Collab	E (GeV)	sqrt(s) (GeV)	Beam	Targets
Fermilab							
Branson	PRL 23, 1331	1977	Princ-Chicago	225	20.5	$\pi-$, $\pi+$, p	C, Sn
Anderson	PRL 42, 944	1979	E444	225	20.5	$\pi-$, $\pi+$, K+, p, ap	C, Cu, W
Abramov	Fermi 91-062-E	1991	E672/E706	530	31.5	$\pi-$	Be
Kartik	PRD 41, 1	1990	E672	530	31.5	$\pi-$	C, AL, Cu, Pb
Katsanevas	PRL 60, 2121	1988	E537	125	15.3	$\pi-$, ap	Be, Cu, W
Akerlof	PR D48, 5067	1993	E537	125	15.3	$\pi-$, ap	Be, Cu, W
Antoniazzi	PRD 46, 4828	1992	E705	300	23.7	$\pi-$, $\pi+$	Li
Gribushin	PR D53, 4723	1995	E672/E706	515	31.1	$\pi-$	Be
Koreshev	PRL 77, 4294	1996	E706/E672	515	31.1	$\pi-$	Be
CERN							
Abolins	PLB 82, 145	1979	WA11/Goliath	150	16.8	$\pi-$	Be
McEwen	PLB 121, 198	1983	WA11	190	18.9	$\pi-$	Be
Badier	Z.Phys. C20, 101	1983	NA3	150	16.8	$\pi-$, $\pi+$, K-, K+, p, ap	H, Pt
"	"	1983	NA3	200	19.4	$\pi-$, $\pi+$, K-, K+, p, ap	H, Pt
"	"	1983	NA3	280	22.9	$\pi-$, $\pi+$, K-, K+, p, ap	H, Pt
Corden	PLB 68, 96	1977	WA39	39.5	8.6	$\pi-$, $\pi+$, K-, K+, p, ap	Cu
Corden	PLB 96, 411	1980	WA39	39.5	8.6	$\pi-$, $\pi+$, K-, K+, p, ap	W
Corden	PLB 98, 220	1981	WA39	39.5	8.6	$\pi-$, $\pi+$, K-, K+, p, ap	p
Corden	PLB 110, 415	1982	WA40	39.5	8.6	$\pi-$, $\pi+$, K-, K+, p, ap	p, W
Alexandrov	NPB 557, 3	1999	Beatrice	350	25.6	$\pi-$	Si, C, W

Large J/ψ cross sections!

COMPASS 2015 NH$_3$ data
Comb. background
J/ψ (MC)
ψ' (MC)
Open-charm (MC)
Drell-Yan (MC)
Total MC + Comb. background

Drell-Yan

COMPASS, PRL 119 (2017) 112002
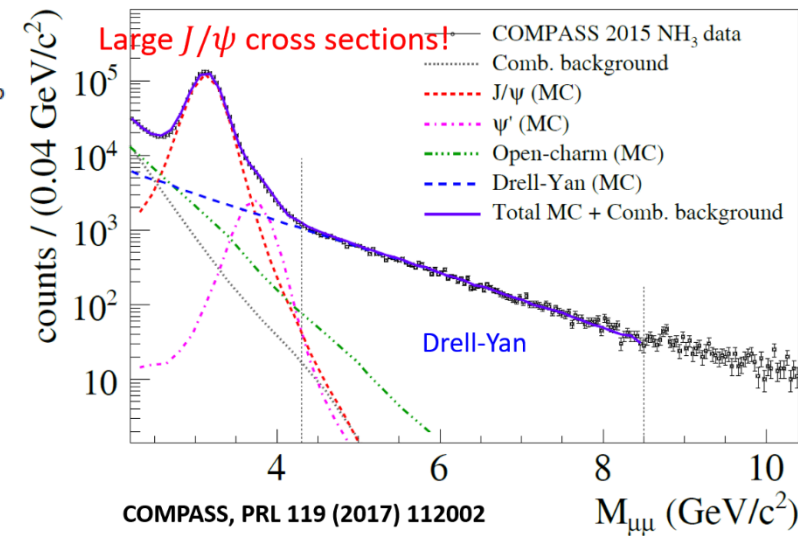
LO & NLO Diagrams of $c\bar{c}$ Production

LO

NLO

A. Petrelli et al./Nuclear Physics B 514 (1998) 245–309

q$\bar{\text{q}}$

D_0

A. Petrelli et al./Nuclear Physics B 514 (1998) 245–309   287
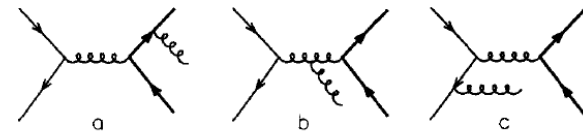
a   b   c

Fig. 8. Diagrams for the real corrections to the $q\bar{q}$ channels. Permutations of outgoing gluons and/or reversal of fermion lines are always implied.

GG

a   b   a

b   a   b

D_1 D_2 D_3
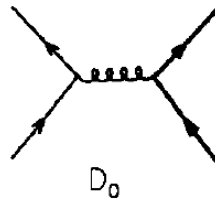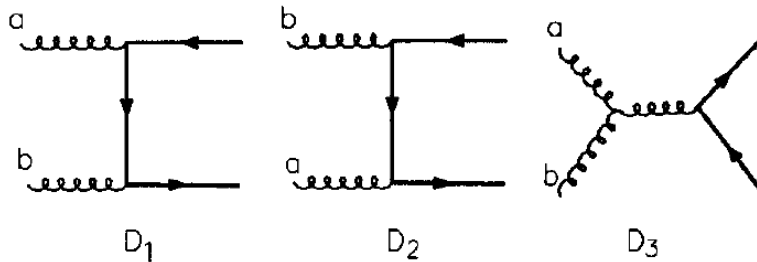
Fig. 2. Diagrams for the $q\bar{q}$ and gg Born amplitudes.

286   A. Petrelli et al./Nuclear Physics B 514 (1998) 245–309
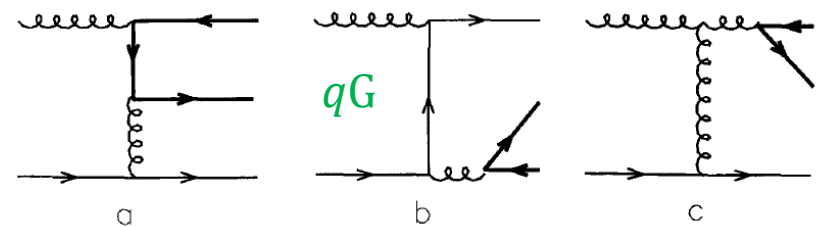
qG

a   b   c

Fig. 7. Diagrams for the gq channels. Reversal of fermion lines is always implied.

10

Model Dependence of $c\bar{c}$ pair Hadronizing

- **Color singlet model (CSM)**: only pairs with matched quantum number of the charmonium.

- **Color evaporation model (CEM)**: all pairs with mass less than $D\bar{D}$ threshold. One hadronization parameter for each charmonium.

- **Non-relativistic QCD model (NRQCD)**: all pairs of different color and spin sates fragmenting with different probabilities – long-distance matrix elements (LDMEs).

Parton emission from a proton (LD)   Hadronization (LD)

p H

perturbative parton process (SD)

p
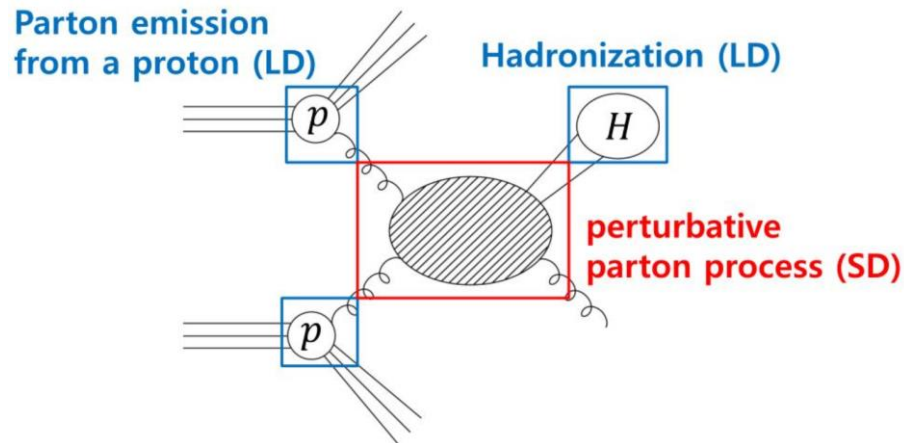
Color evaporation model (CEM)

[Phys. Rev. D 102, 054024 (2020)](#); [arXiv: 2006.06947](#)

Constraining gluon density of pions at large x by pion-induced J/ψ production

Wen-Chen Chang

Institute of Physics, Academia Sinica, Taipei 11529, Taiwan

Jen-Chieh Peng

Department of Physics, University of Illinois at Urbana-Champaign, Urbana, Illinois 61801, USA

Stephane Platchkov

IRFU, CEA, Université Paris-Saclay, 91191 Gif-sur-Yvette, France
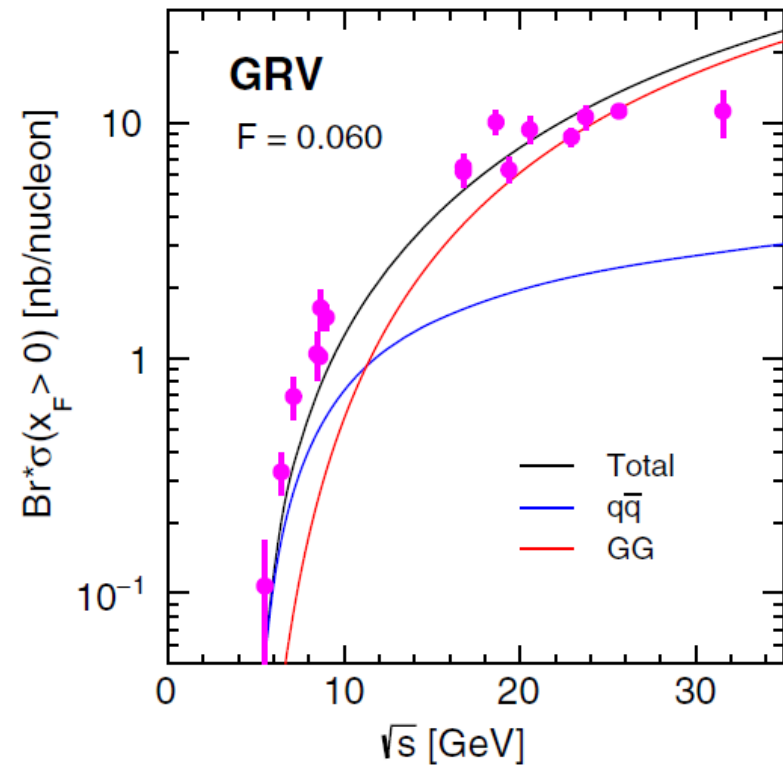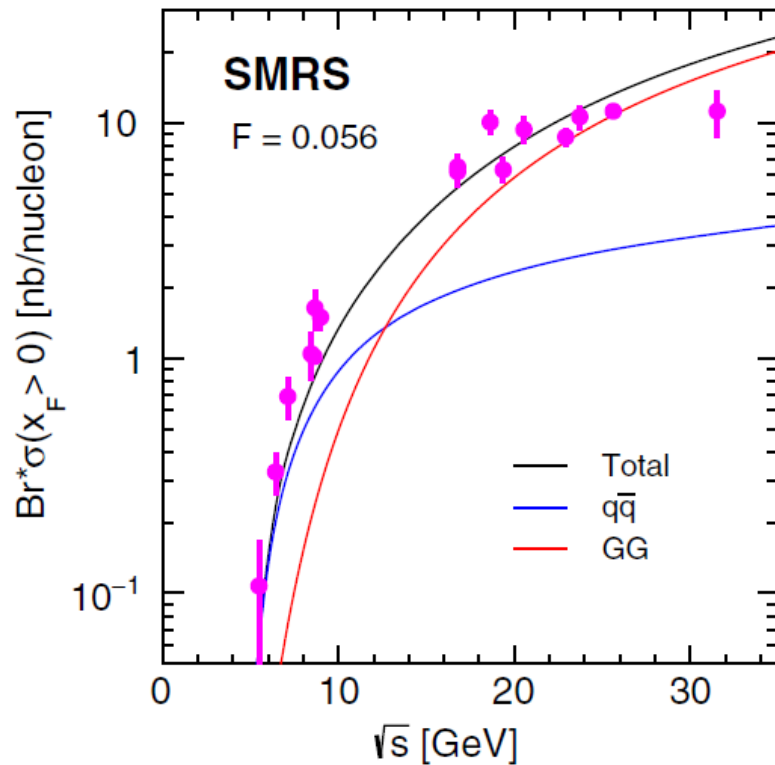
Takahiro Sawada

*Department of Physics, Osaka City University, Osaka 558-8585, Japan*

The gluon distributions of the pion obtained from various global fits exhibit large variations among them. Within the framework of the color evaporation model, we show that the existing pion-induced J/ψ
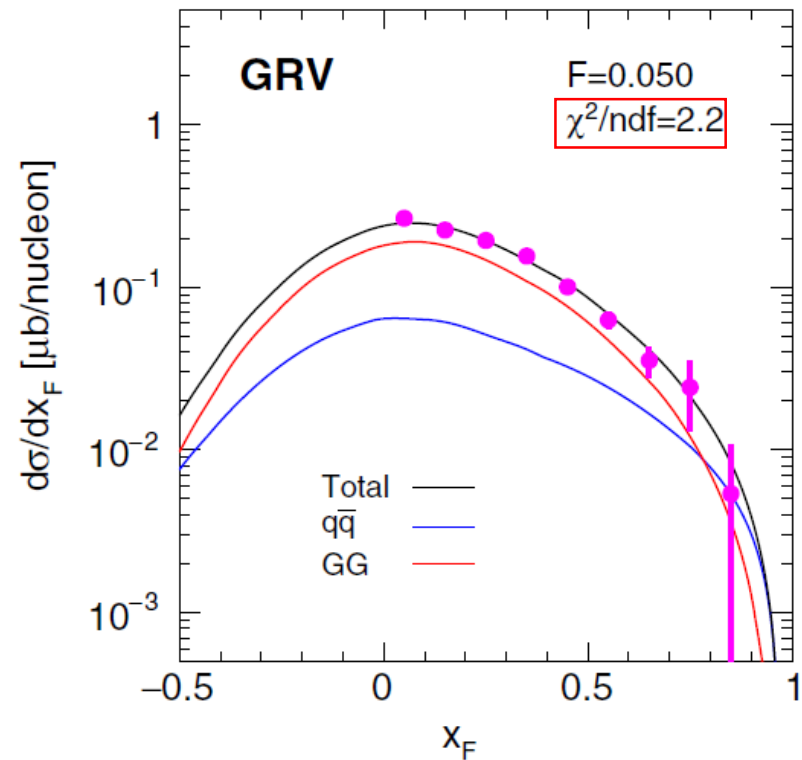
Data vs. CEM NLO
: Energy dependence

GG dominates at high energies, while $q\bar{q}$ is important near threshold.
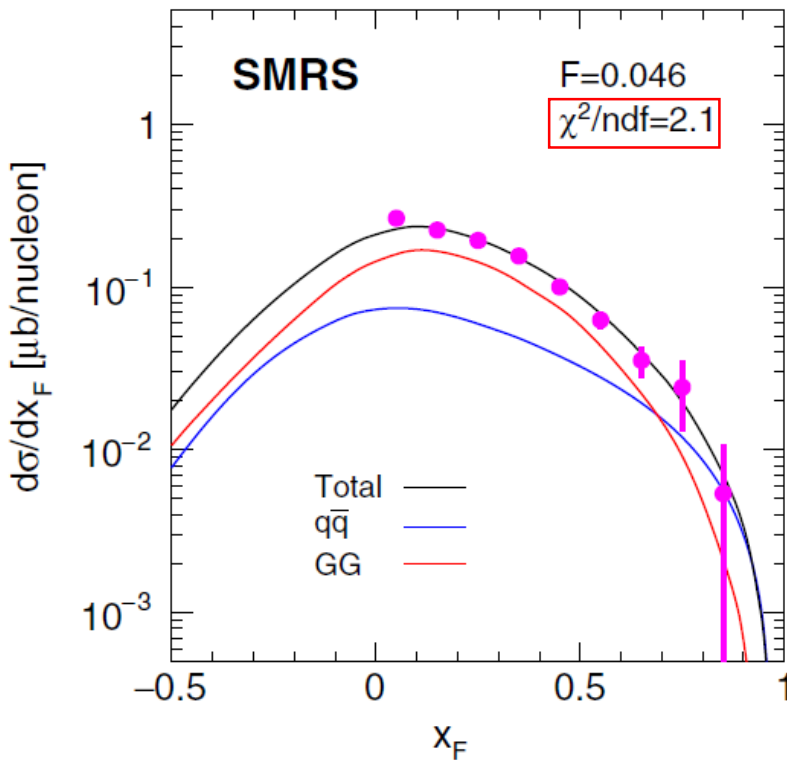
Data vs. CEM NLO
: Energy dependence
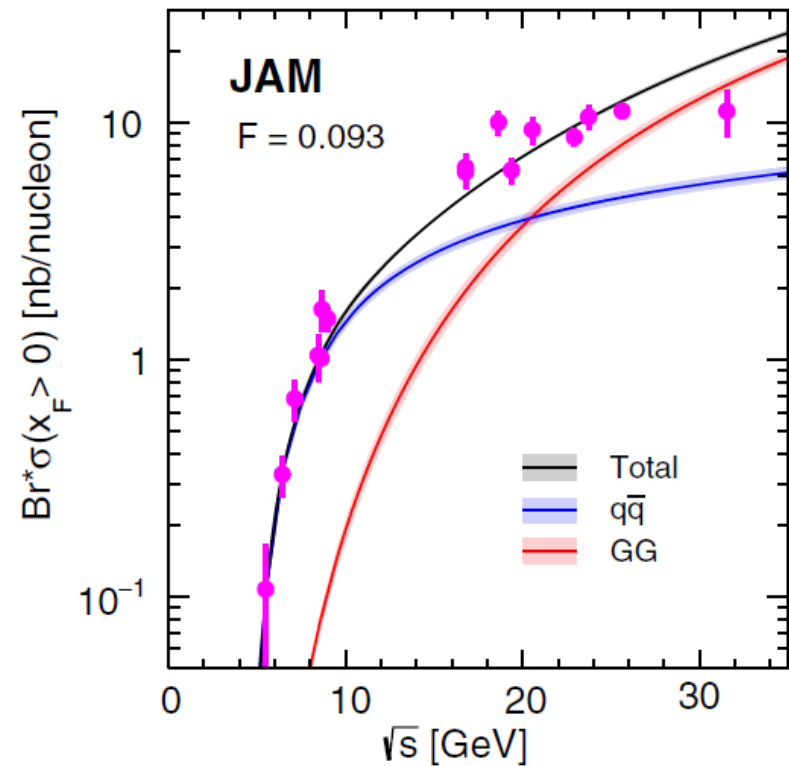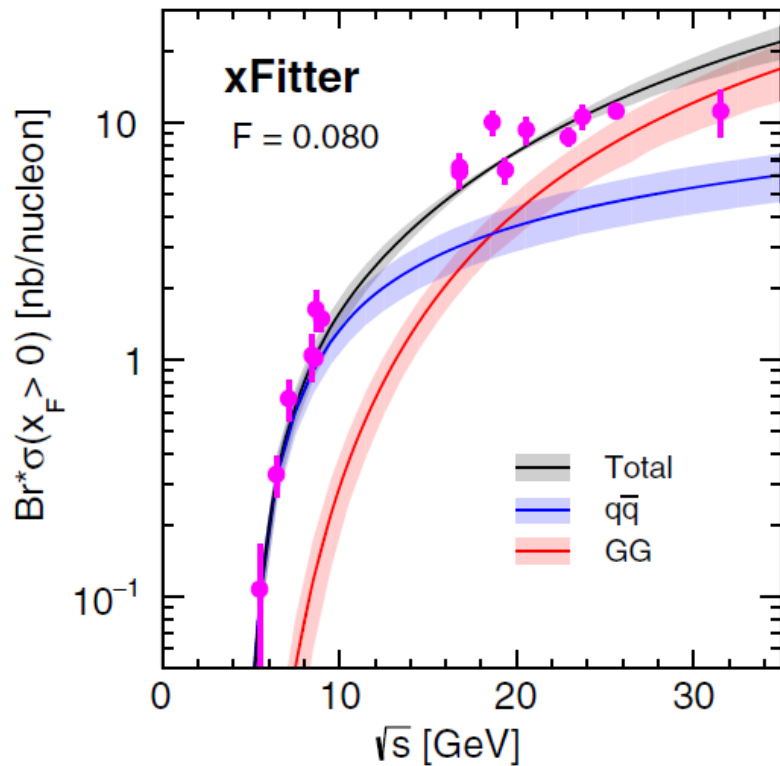
GG dominates at high energies, while $q\bar{q}$ is important near threshold.

Data vs. CEM NLO
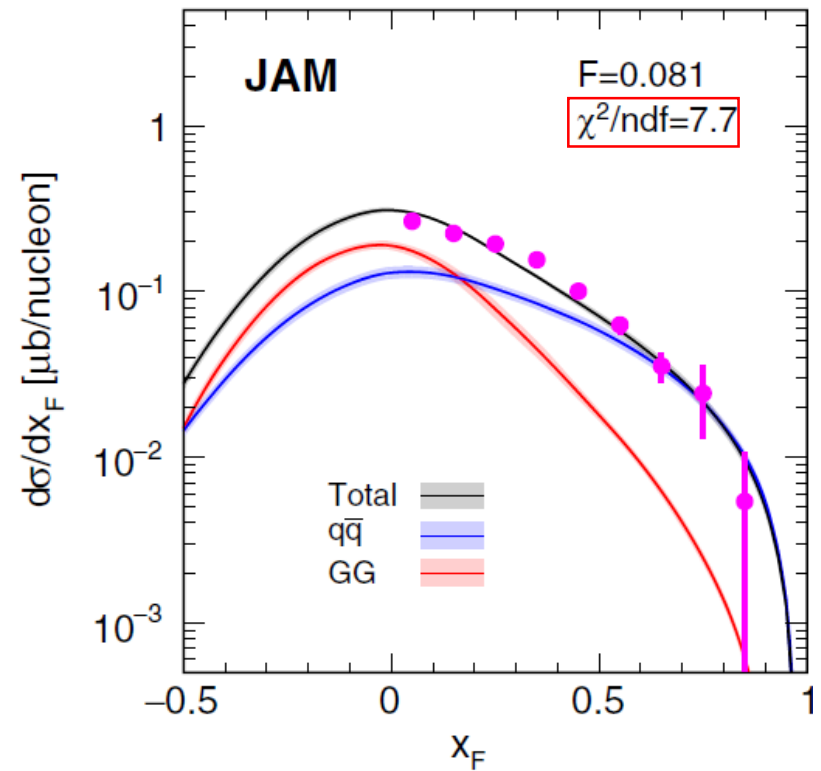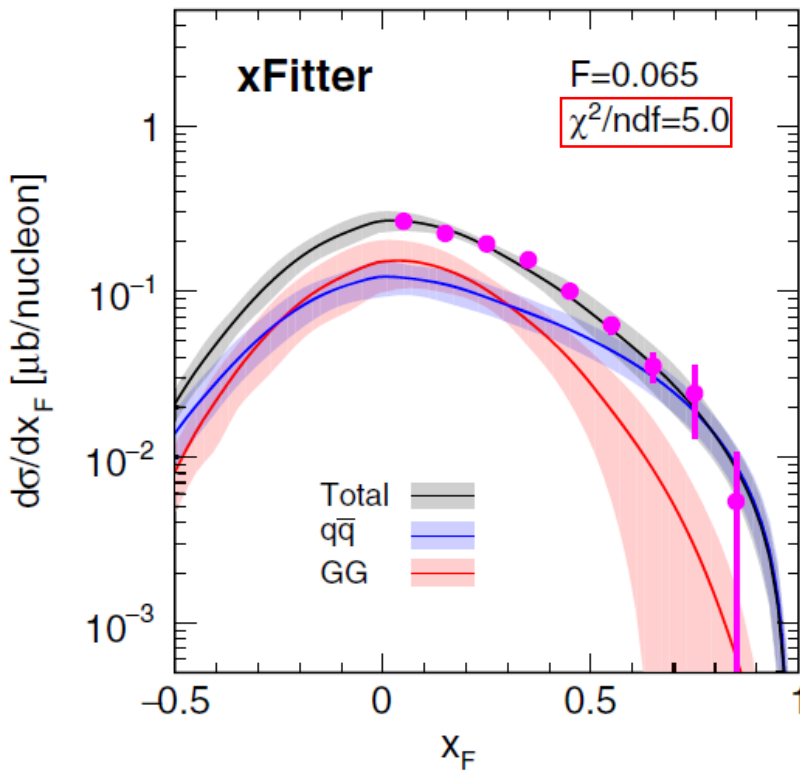## [$\pi^- + Pt \to Jpsi + X$ at **200 GeV**, Z. Phys. C20,101(1983)]

- The GG contribution dominates except at very forward or backward directions.
- To well describe the data for xF>0.2, an appropriate weighting of GG and $q\bar{q}$ contributions is necessary.

Data vs. CEM NLO

$[\pi^- + Pt \to Jpsi + X$ **at 200 GeV**, Z. Phys. C20,101(1983)]

- The GG contribution dominates except at very forward or backward directions.
- To well describe the data for xF>0.2, an appropriate weighting of GG and $q\bar{q}$ contributions is necessary.

Data vs. CEM Calculations

TABLE III. Results of F factor and χ^2/ndf value of the best fit of the NLO CEM calculations for SMRS, GRV, xFitter, and JAM pion PDFs to the data listed in Table II. The F^* factor and χ^2/ndf^* are the ones corresponding to the fit with inclusion of PDF uncertainties for xFitter and JAM.

Data	SMRS		GRV		xFitter				JAM			
Experiment (P_{beam})	F	χ^2/ndf	F	χ^2/ndf	F	F^*	χ^2/ndf	χ^2/ndf^*	F	F^*	χ^2/ndf	χ^2/ndf^*
E672, E706 (515)	0.040	1.2	0.040	2.2	0.063	0.063	6.8	4.7	0.081	0.081	18.9	18.5
E705 (300)	0.052	2.3	0.053	1.9	0.073	0.076	3.2	1.3	0.086	0.086	16.1	15.9
NA3 (280)	0.046	1.5	0.049	2.0	0.067	0.069	5.0	3.2	0.081	0.081	10.4	10.3
NA3 (200)	0.046	2.1	0.050	2.2	0.065	0.066	5.0	1.3	0.081	0.081	7.7	7.6
WA11 (190)	0.054	5.0	0.058	7.2	0.078	0.076	19.4	6.2	0.091	0.091	73.7	72.9
NA3 (150)	0.065	1.1	0.071	1.0	0.089	0.091	2.6	1.6	0.108	0.108	3.9	3.8
E537 (125)	0.044	1.5	0.049	1.5	0.065	0.065	3.1	1.4	0.083	0.083	3.5	3.5
WA39 (39.5)	0.068	1.3	0.079	1.4	0.073	0.072	1.1	0.8	0.080	0.080	1.2	1.2

- The hadronization F factor is stable across energy.
- High-energy J/ψ data have a large sensitivity to the large-x gluon density of pions.
- The valence-quark distributions plays a minor role if away from the threshold.
- **CEM NLO calculations favor SMRS and GRV PDFs whose gluon densities at x > 0.1 are higher, compared with xFitter and JAM PDFs.**

Are these observations model dependent?

Non-relativistic QCD model (NRQCD) [arXiv: 2103.11660](#)

NRQCD analysis of charmonium production with pion and proton beams at fixed-target energies

Chia-Yu Hsieh,[a,b,1] Yu-Shiang Lian[a,c,1] Wen-Chen Chang,[a] Jen-Chieh Peng,[d] Stephane Platchkov[e] and Takahiro Sawada[f]

[a] Institute of Physics, Academia Sinica, Taipei 11529, Taiwan
[b] Department of Physics, National Central University, 300 Jhongda Road, Jhongli 32001, Taiwan.
[c] Department of Physics, National Kaohsiung Normal University, Kaohsiung County 824, Taiwan
[d] Department of Physics, University of Illinois at Urbana-Champaign, Urbana, Illinois 61801, USA
[e] IRFU, CEA, Université Paris-Saclay, 91191 Gif-sur-Yvette, France
[f] Department of Physics, Osaka City University, Osaka 558-8585, Japan

E-mail: cyhsieh@phys.sinica.edu.tw, yslian@gate.sinica.edu.tw, changwc@phys.sinica.edu.tw, jcpeng@illinois.edu, Stephane.Platchkov@cern.ch, tsawada@sci.osaka-cu.ac.jp

ABSTRACT: We present an analysis of hadroproduction of J/ψ and $\psi(2S)$ at fixed-target energies in the framework of non-relativistic QCD (NRQCD). Using both pion- and proton-induced data, a new determination of the color-octet long-distance matrix elements (LDMEs) is obtained. Compared with previous results, the contributions from the $q\bar{q}$ and color-octet processes are significantly enhanced, especially at lower energies. A good agreement between the pion-induced J/ψ production data and NRQCD calculations using the newly obtained LDMEs is achieved. We find that the pion-induced charmonium production data are sensitive to the gluon density of pions, and favor pion PDFs with relatively large gluon contents at large x.
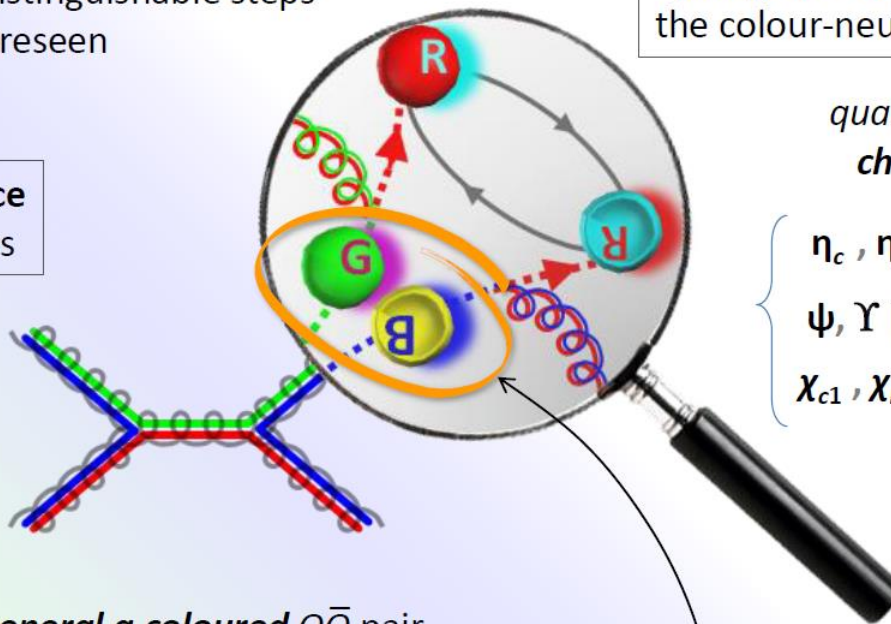
NRQCD

The "cascade" (*factorization*) approach of NRQCD
Non-Relativistic

For **heavy** quarkonia
two distinguishable steps
are foreseen

2) long-distance evolution to
the colour-neutral bound state

*quantum numbers
change* to final

1) short-distance
partonic process

η_c , η_b $[^1S_0]$

ψ, Υ $[^3S_1]$ χ_{c0} , χ_{b0} $[^3P_0]$

χ_{c1} , χ_{b1} $[^3P_1]$ χ_{c2} , χ_{b2} $[^3P_2]$

produces *in general a coloured* $Q\bar{Q}$ pair
of any $^{2S+1}L_J$ *quantum numbers*

$^1S_0$ $^1S_0$ $^3S_1$ $^3P_0$ $^3P_2$
$^1D_2$ $^3P_2$ $^3D_3$ $^1P_1$ $^3S_1$
$^3P_1$ $^3D_2$ $^3D_1$ $^3P_1$ $^1P_1$

Even if the *pre-resonance* $Q\bar{Q}$ state
is not observed, it determines,
with its own quantum properties,
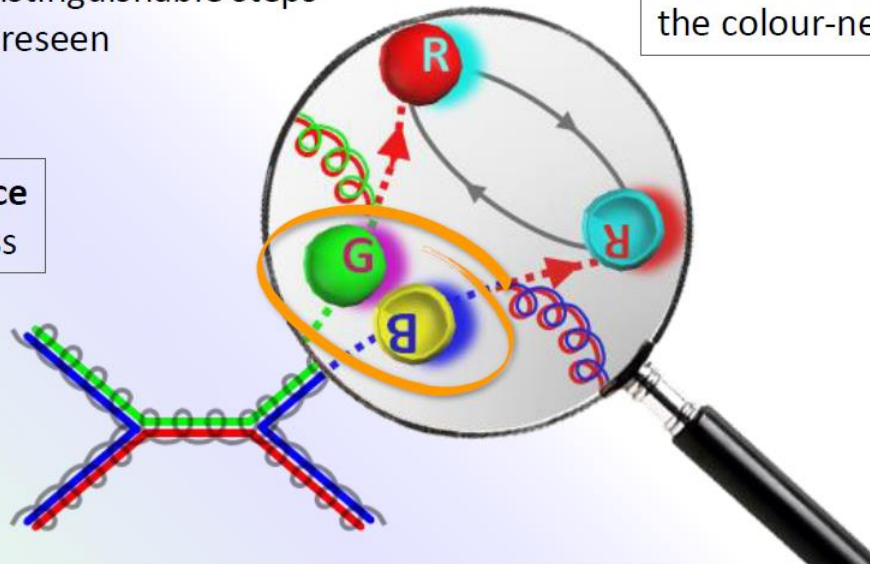the observable kinematics and *polarization*

19

NRQCD

The "cascade" (*factorization*) approach of NRQCD

For **heavy** quarkonia
two distinguishable steps
are foreseen

2) **long-distance** evolution to
the colour-neutral bound state

1) **short-distance**
partonic process

1) *short-distance coefficients* (**SDCs**):
p_T-dependent partonic cross sections

2) *long-distance matrix elements* (**LDMEs**):
constant, **fitted from data**

$$\sigma(A + B \rightarrow \mathcal{Q} + X) = \sum_{S, L, C} \mathcal{S}\{A + B \rightarrow (Q\bar{Q})_C[^{2S+1}L_J] + X\} \cdot \mathcal{L}\{(Q\bar{Q})_C[^{2S+1}L_J] \rightarrow \mathcal{Q}\}$$

$Q\bar{Q}$ **angular momentum**
and **colour** configurations

20

NRQCD Framework
PRD 54, 2005 (1996)

Hadroproduction of quarkonium in fixed-target experiments

M. Beneke

Stanford Linear Accelerator Center, Stanford University, Stanford, California 94309

I. Z. Rothstein

University of California, San Diego, 9500 Gilman Drive, La Jolla, California 92093

(Received 25 March 1996)

We analyze charmonium and bottomonium production at fixed-target experiments. We find that the inclusion of color octet production channels removes large discrepancies between experiment and the predictions of the color singlet model for the total production cross section. Furthermore, including octet contributions accounts for the observed direct to total J/ψ production ratio. As found earlier for photoproduction of quarkonia, a fit to fixed-target data requires smaller color octet matrix elements than those extracted from high-p_t production at the Fermilab Tevatron. We argue that this difference can be explained by systematic differences in the velocity expansion for collider and fixed-target predictions. While the color octet mechanism thus appears to be an essential part of a satisfactory description of fixed-target data, important discrepancies remain for the χ_{c1}/χ_{c2} production ratio and J/ψ (ψ') polarization. These discrepancies, as well as the differences between pion- and proton-induced collisions, emphasize the need for including higher twist effects in addition to the color octet mechanism. [S0556-2821(96)05515-4]

PACS number(s): 13.85.Ni, 13.88.+e, 14.40.Gx

Long-Distance Matrix Elements (LDMEs) PRD 54, 2005 (1996)

$\left\langle O_{1,8}^{H}\left[{}^{2S+1}L_{J}\right]\right\rangle$

	$J/\psi,\ \psi(2S)$	χ_{c0}	χ_{c1}	χ_{c2}
$q\bar{q}$	$\langle\mathcal{O}_8^H[{}^3S_1]\rangle$	$\langle\mathcal{O}_8^H[{}^3S_1]\rangle$	$\langle\mathcal{O}_8^H[{}^3S_1]\rangle$	$\langle\mathcal{O}_8^H[{}^3S_1]\rangle$
GG	$\langle\mathcal{O}_1^H[{}^3S_1]\rangle$ Δ_8^*	$\langle\mathcal{O}_1^H[{}^3P_0]\rangle$	$\langle\mathcal{O}_1^H[{}^3P_1]\rangle$	$\langle\mathcal{O}_1^H[{}^3P_2]\rangle$
qG			$\langle\mathcal{O}_1^H[{}^3P_1]\rangle$	

$$\Delta_8 = \langle\mathcal{O}_8^H[{}^1S_0]\rangle + \frac{3}{m_c^2}\langle\mathcal{O}_8^H[{}^3P_0]\rangle + \frac{4}{5m_c^2}\langle\mathcal{O}_8^H[{}^3P_2]\rangle$$

H	$\langle\mathcal{O}_1^H[{}^3S_1]\rangle$	$\langle\mathcal{O}_1^H[{}^3P_0]\rangle/m_c^2$	$\langle\mathcal{O}_8^H[{}^3S_1]\rangle$	$\langle\mathcal{O}_8^H[{}^1S_0]\rangle=\langle\mathcal{O}_8^H[{}^3P_0]\rangle/m_c^2$
J/ψ	1.16		6.6×10^{-3}	3.75×10^{-3}
$\psi(2S)$	0.76		4.6×10^{-3}	0.65×10^{-3}
χ_{c0}		0.044	3.2×10^{-3}	

Determined by fit of proton- and pion-indcued data

color-singlet (CS) LDMEs   color-octet (CO) LDMEs

$$\sigma_{J/\psi} = \sigma_{J/\psi}^{direct} + Br(\psi(2S)\to J/\psi X)\sigma_{\psi(2S)} + \sum_{J=0}^{2} Br(\chi_{cJ}\to J/\psi\gamma)\sigma_{\chi_{cJ}}$$

Jpsi/psi' Data vs. NRQCD
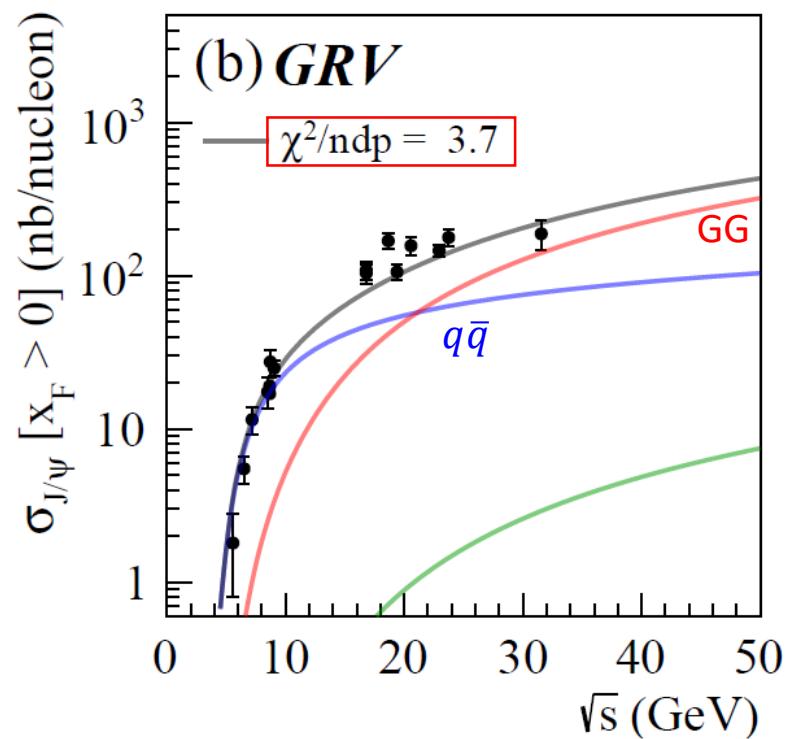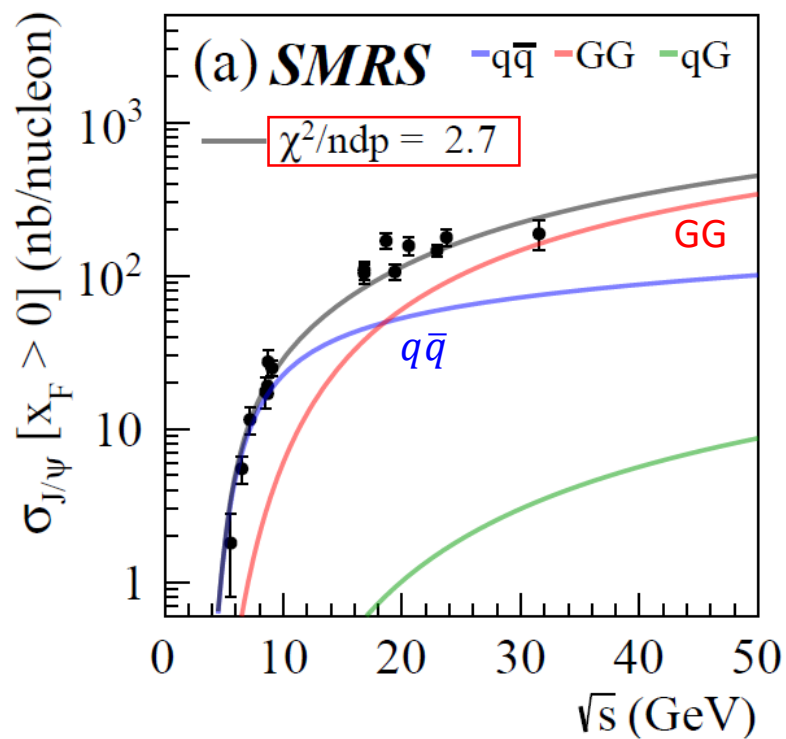
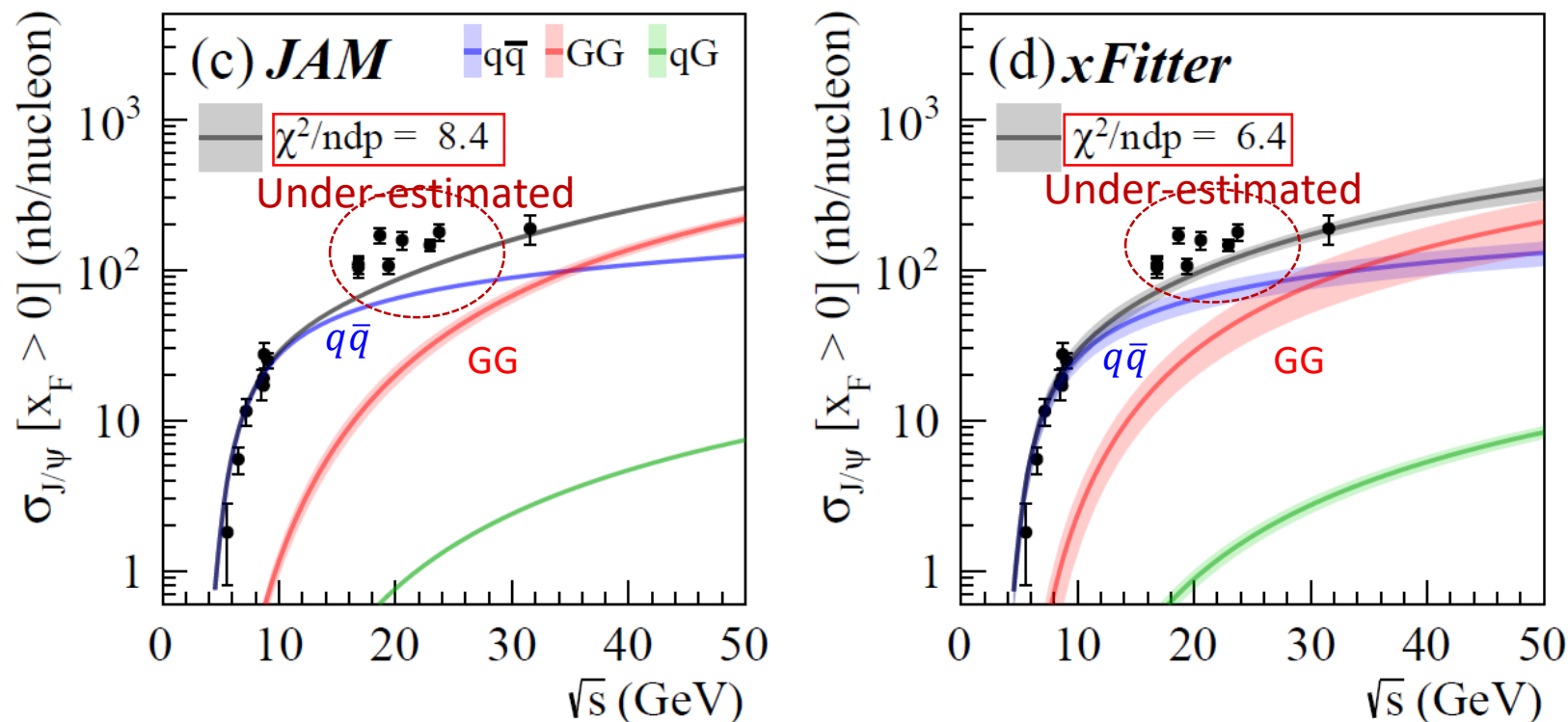Best-fitted CO [3S1] and [1S0] LDMEs by p+N Jpsi/psi' and π^-+N Jpsi/psi' data.

$\langle \mathcal{O}_8^{J/\psi}[^3S_1] \rangle$	6.6×10^{-3}	$(1.47 \pm 0.07) \times 10^{-1}$	$(9.5 \pm 0.4) \times 10^{-2}$
$\langle \mathcal{O}_8^{J/\psi}[^1S_0] \rangle^*$	3.75×10^{-3}	$(0 \pm 1) \times 10^{-4}$	$(2.2 \pm 0.3) \times 10^{-3}$
$\langle \mathcal{O}_8^{\psi(2S)}[^3S_1] \rangle$	4.6×10^{-3}	$(2.5 \pm 0.2) \times 10^{-2}$	$(2.6 \pm 0.2) \times 10^{-2}$
$\langle \mathcal{O}_8^{\psi(2S)}[^1S_0] \rangle^*$	6.5×10^{-4}	$(0 \pm 1) \times 10^{-4}$	$(5 \pm 8) \times 10^{-5}$

π^-+N→Jpsi+X: pion PDFs

$\pi^- + N \rightarrow$ Jpsi+X: pion PDFs

- The dependence of best-fit LDMEs to the pion PDFs is mild.
- The deficiency of JAM and xFitter in the GG contributions generates a relatively large χ^2 in the description of data.

Data vs. NRQCD

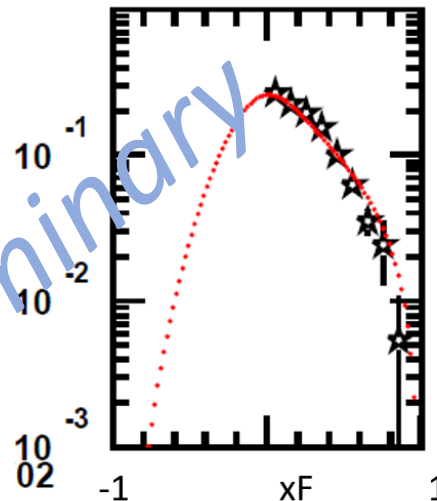$[\pi^- + Pt \rightarrow Jpsi + X$ at **200 GeV**, Z. Phys. C20,101(1983)]
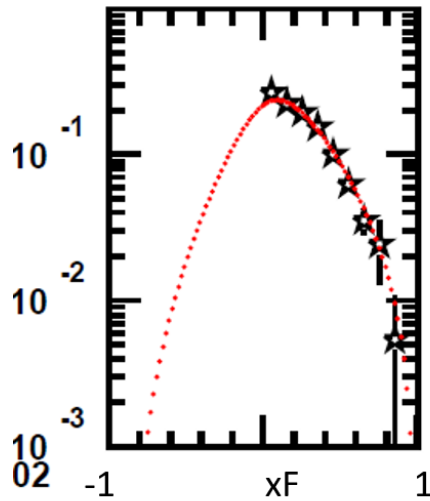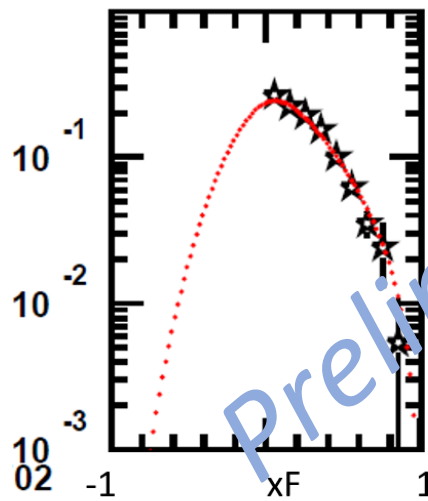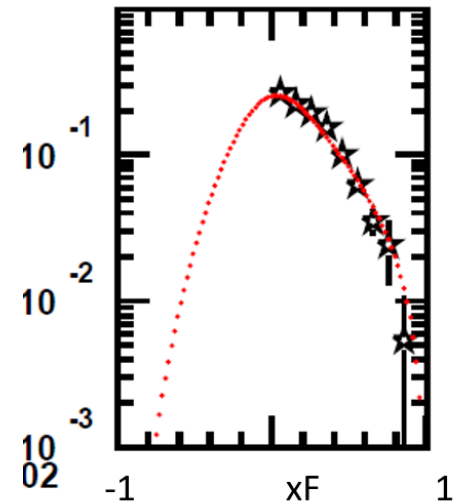
SMRS	GRV	JAM	xFitter
$\chi^2 = 37.9/10 = 3.8$	$\chi^2 = 69.0/10 = 6.9$	$\chi^2 = 125.8/10 = 12.6$	$\chi^2 = 115.8/10 = 11.6$

SMRS & GRV provide a better description of data than JAM and xFitter.

Summary

- The pion PDFs have been determined by the Drell-Yan, direct photon, J/psi and recently leading-neutron data. Nevertheless discrepancy of valence quark and gluon densities at x>0.1 is seen.

- Within CEM and NRQCD, the high-energy J/psi data are shown to be sensitive to the pion gluon distribution. The current data favor the SMRS and GRV pion PDFs, containing relatively larger gluon content at large x.

- The future pion(kaon)-induced charmonium data from COMPASS and AMBER shall provide strong constrains on the large-x gluon distributions of pions (kaons).

Backup

Data vs. CEM LO/NLO

$[\pi^- + Be \to Jpsi + X$ at **515 GeV**, PRD 53, 4723 (1996)]

m_c=1.5 GeV, μ_F=2m_c, μ_R=m_c,
hadronization parameter F determined by the fit.
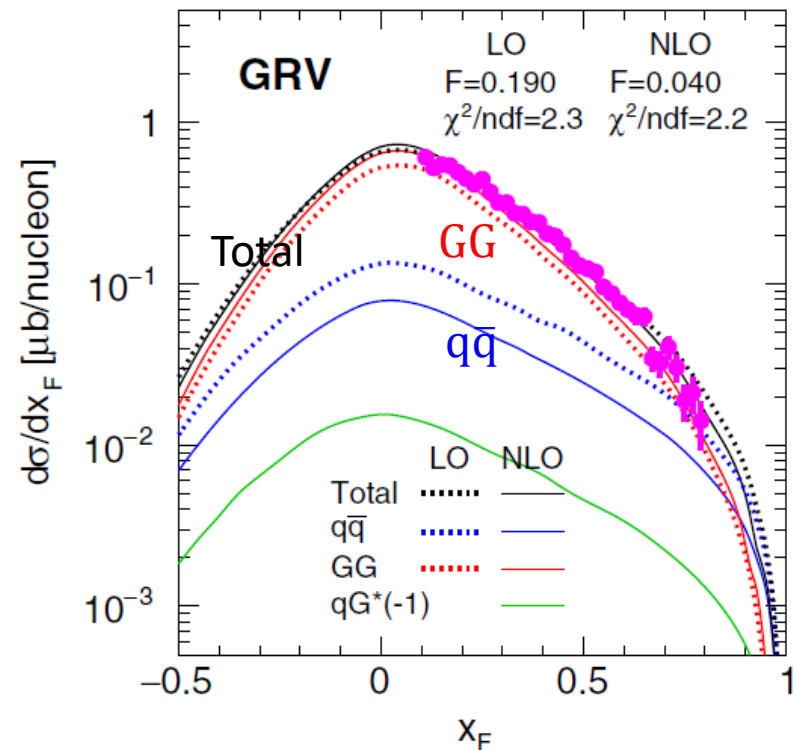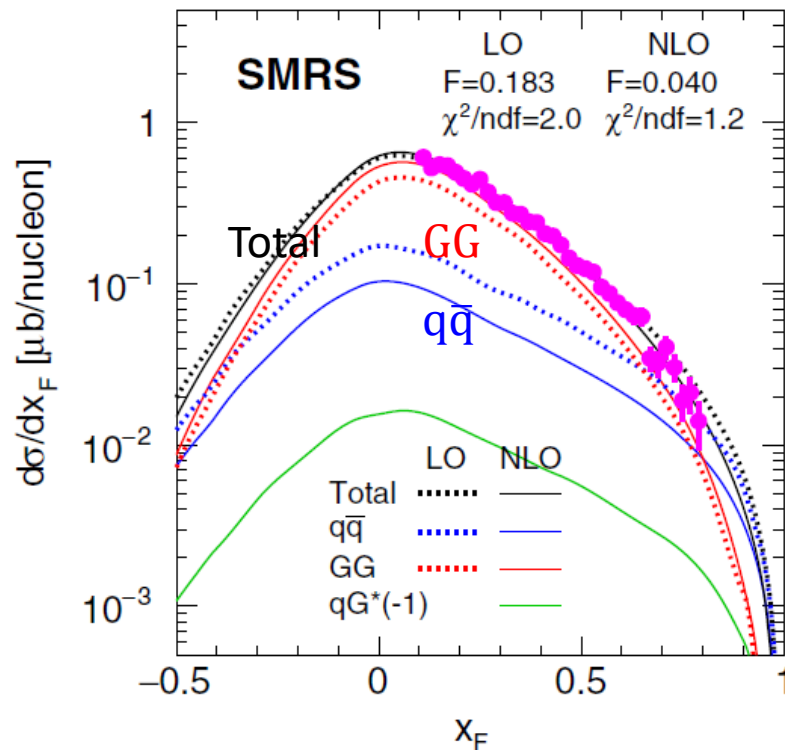
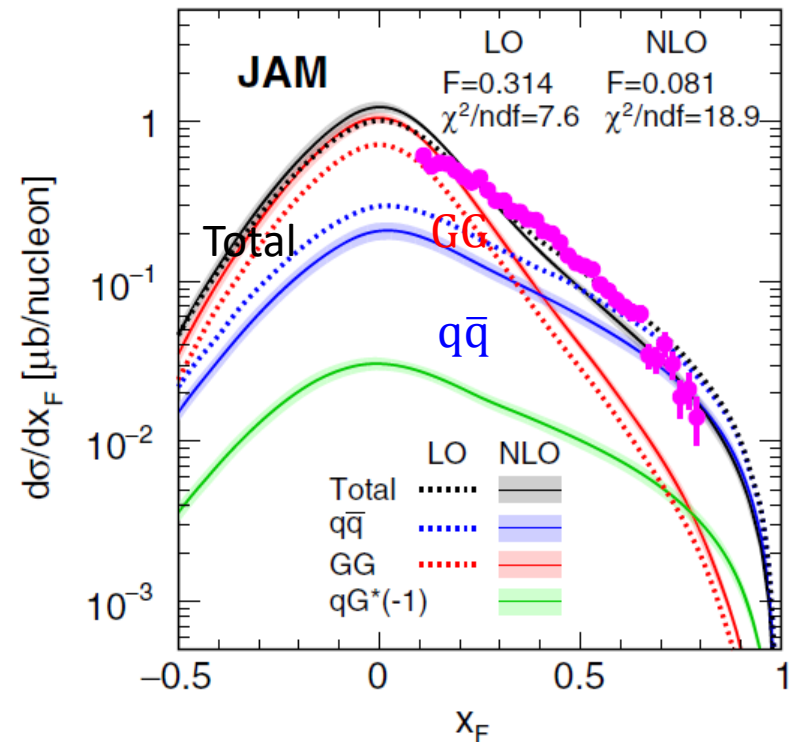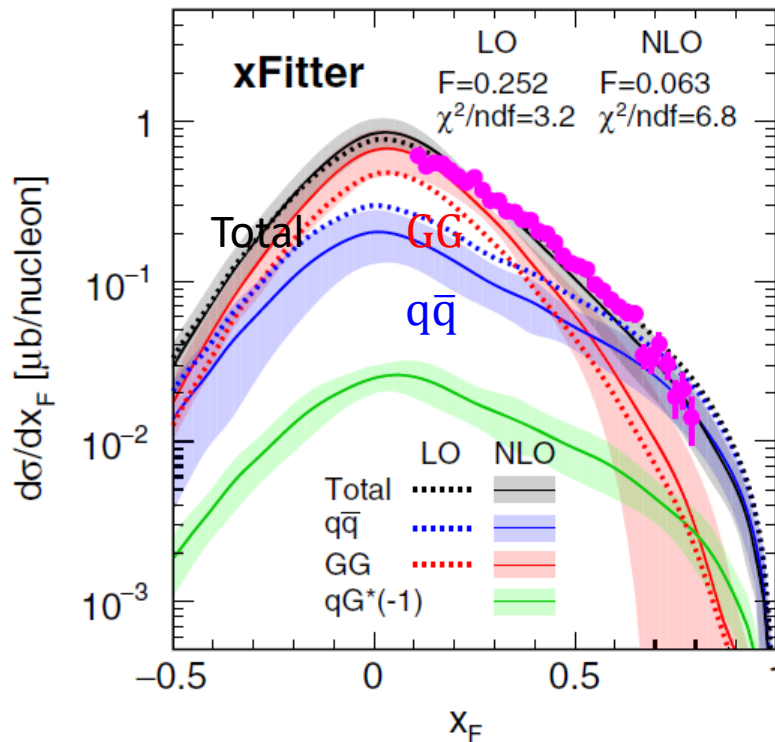
- The GG contribution dominates except at very forward or backward directions.
- The weighting of GG contribution is enhanced in the NLO calculations.

Data vs. CEM LO/NLO

[$\pi^- + Be \rightarrow Jpsi + X$ at 515 GeV, PRD 53, 4723 (1996)]

m_c=1.5 GeV, μ_F=2m_c, μ_R=m_c,
hadronization parameter F determined by the fit.

- The GG contribution dominates except at very forward or backward directions.
- The weighting of GG contribution is enhanced in the NLO calculations.
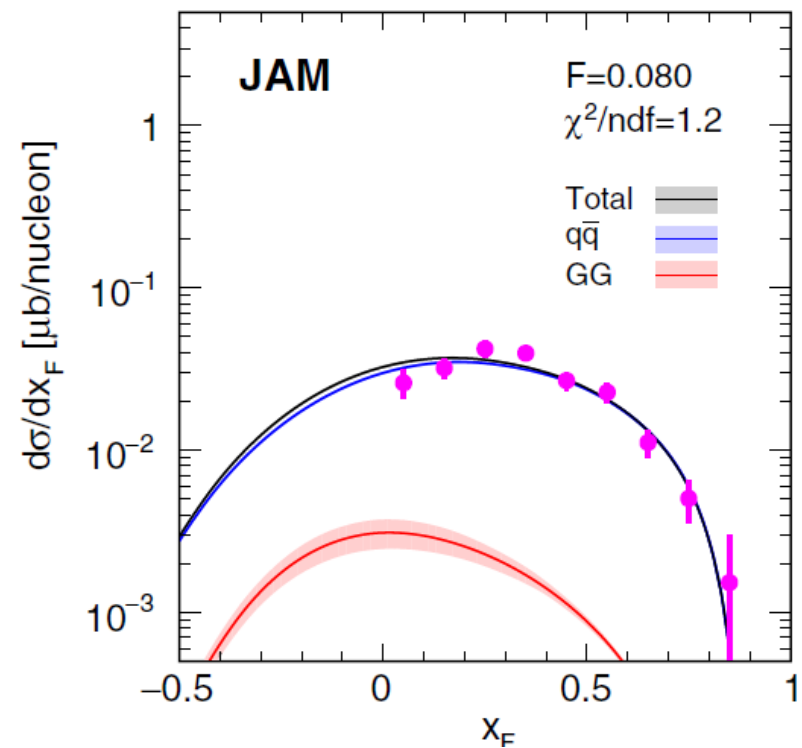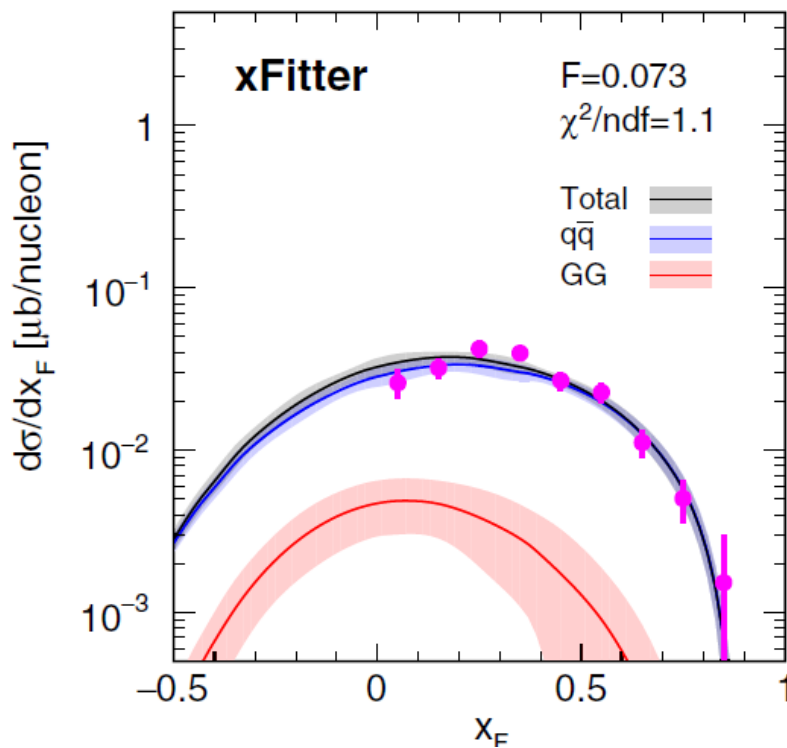
Data vs. CEM NLO

$[\pi^- + p \to Jpsi + X$ **at 39.5 GeV, PLB 98, 220 (1981)]**
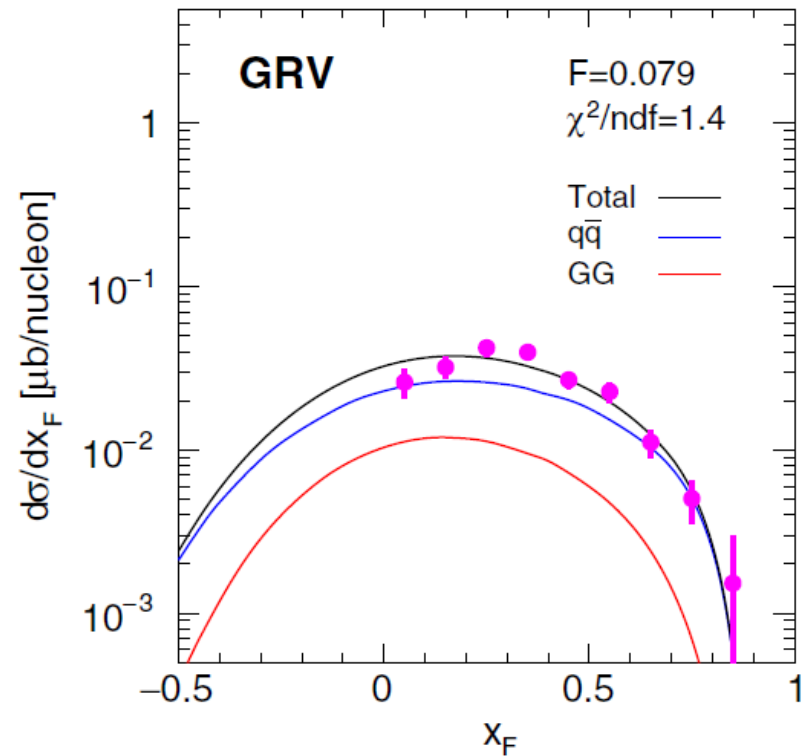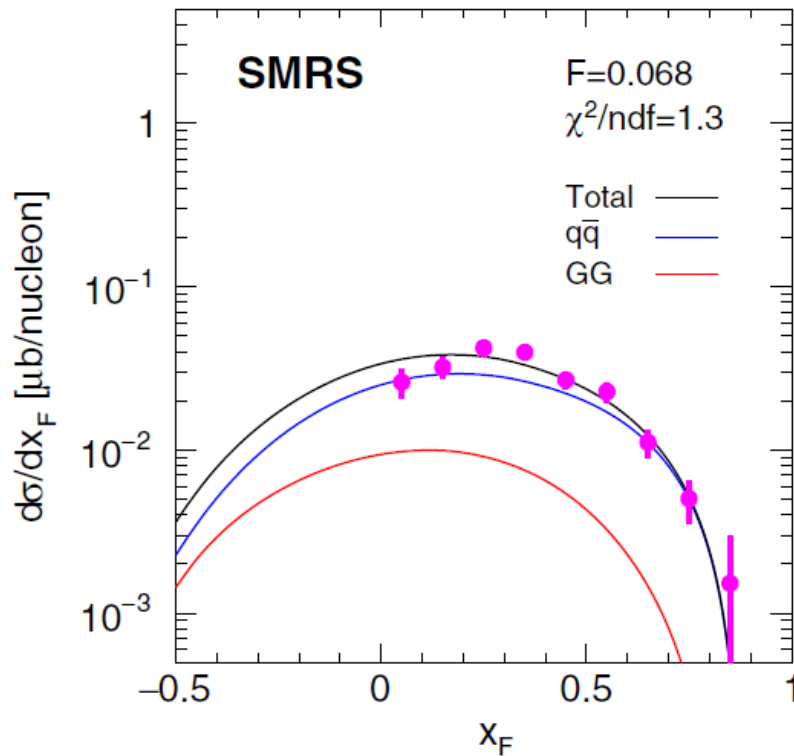
- Calculations of all four PDFs describe the data well.

Data vs. CEM NLO
$[\pi^- + p \to Jpsi + X$ at **39.5 GeV**, **PLB 98, 220 (1981)]**

- Calculations of all four PDFs describe the data well.

Beneke & Roshstein,
PRD 54, 2005 (1996)

The poor description of the pion-induced data was speculated due to the poor pion PDFs or higher twist effects.
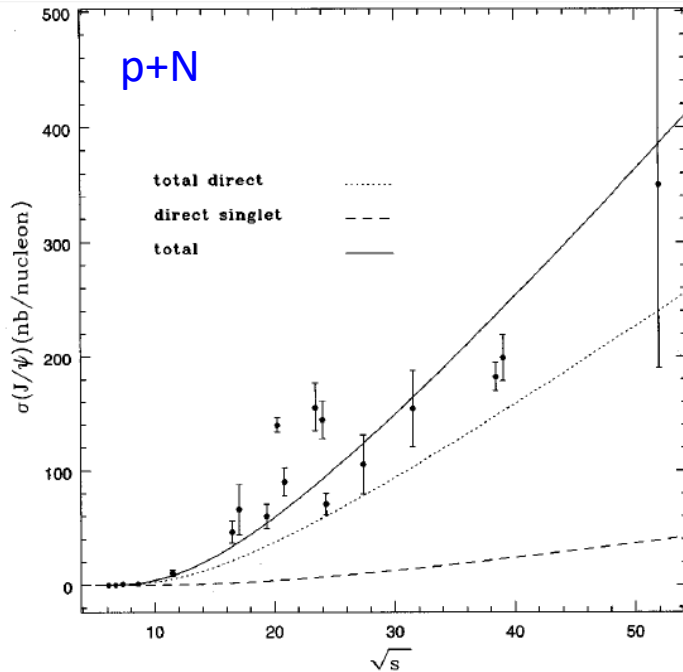

FIG. 2. J/ψ production cross sections in proton-nucleon collisions for $x_F > 0$. The dotted line is the direct J/ψ production rate in the CSM and the dashed line includes the contribution from the color octet processes. The total cross section (solid line) includes radiative feeddown from the χ_{cJ} and ψ' states. The solid line is obtained with $\Delta_8(J/\psi) = 3.0 \times 10^{-2}$ GeV^3.
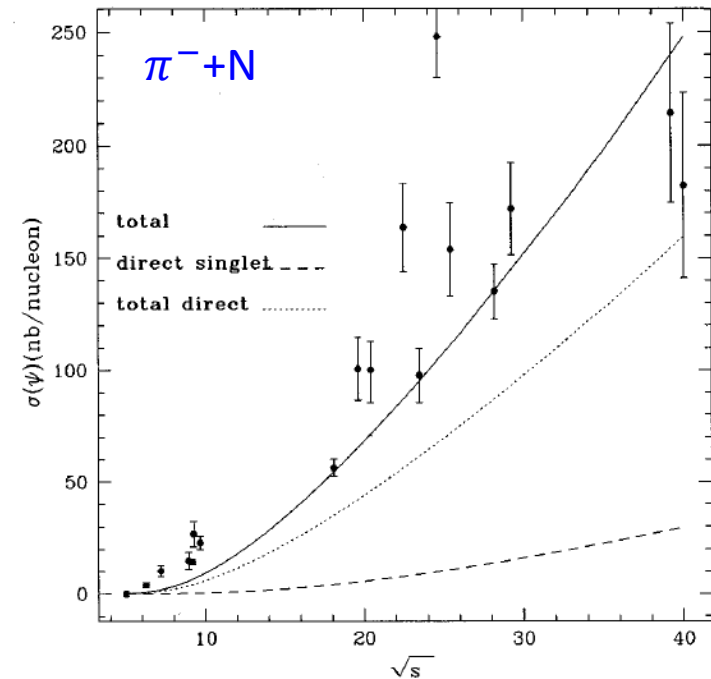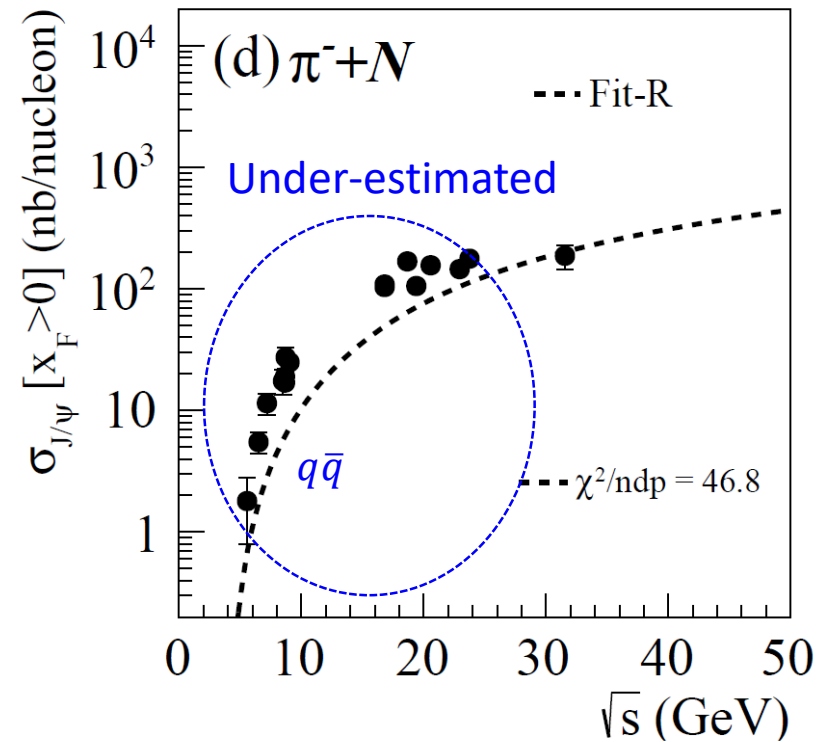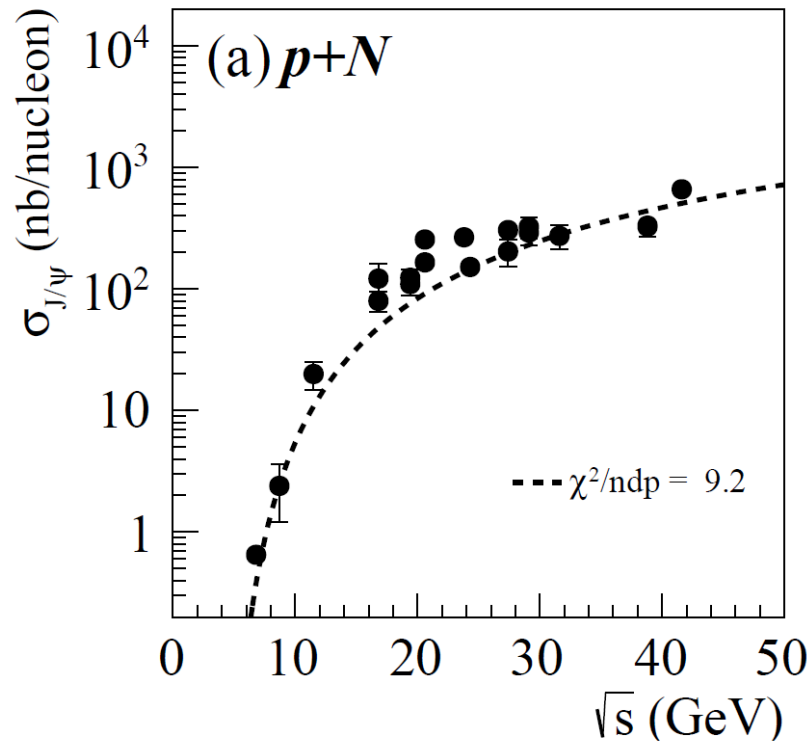
FIG. 5. J/ψ production cross sections in pion-nucleon collisions for $x_F > 0$. Direct J/ψ production in the CSM (dashed line) and after inclusion of color octet processes (dotted line). The total cross section (solid line) includes radiative feeddown from the χ_{cJ} and ψ' states. The solid line is obtained with $\Delta_8(J/\psi) = 3.0 \times 10^{-2}$ GeV^3.
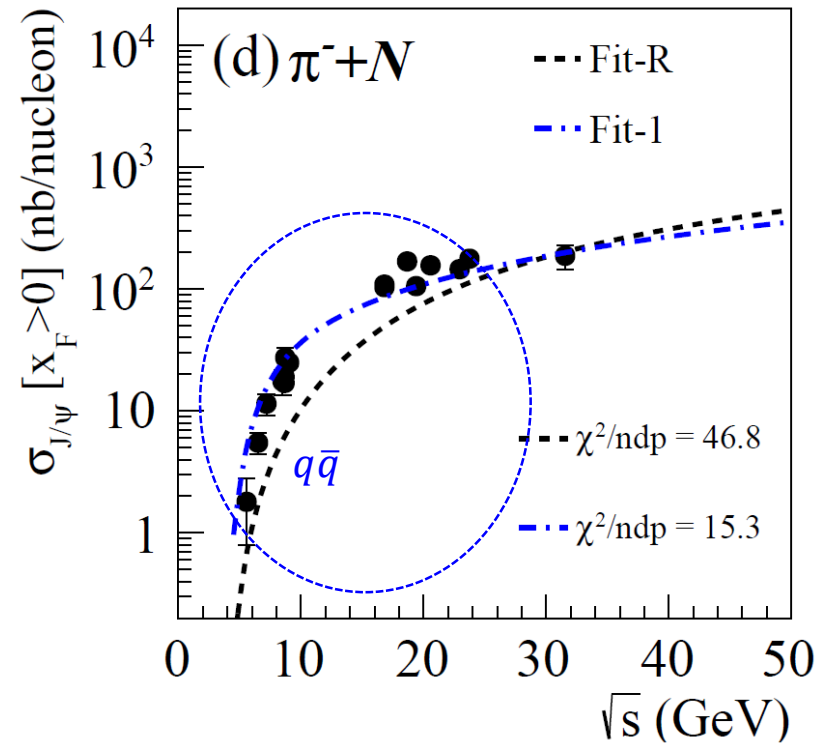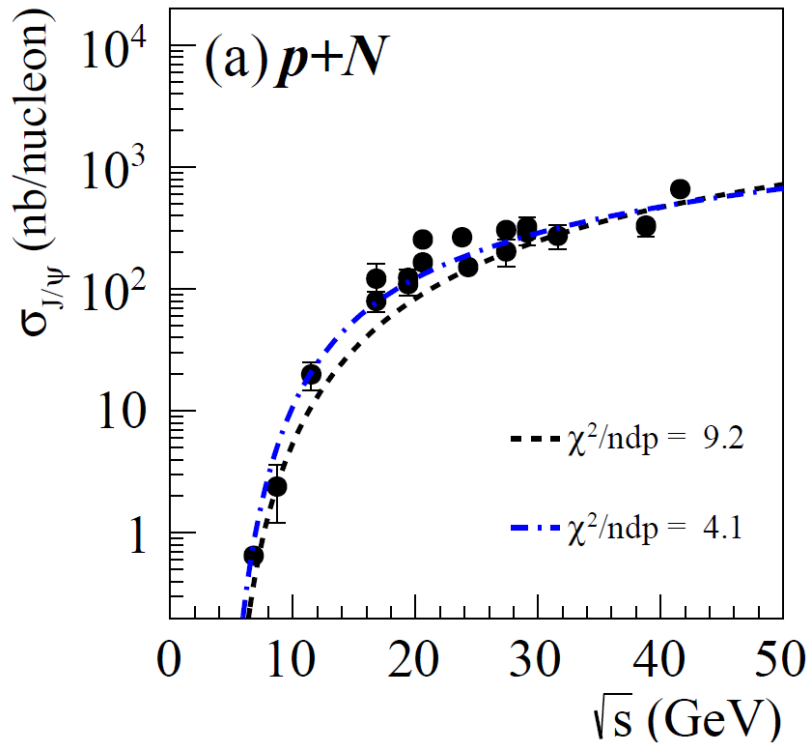
33

Jpsi Data vs. NRQCD: Fit-R

- Fit by p+N Jpsi/psi' data
- Best-fit CO [1S0] LDMEs from Beneke & Roshstein

		$q\bar{q}$	
$\langle \mathcal{O}_8^{J/\psi}[^3S_1] \rangle$	6.6×10^{-3}	$(1.47 \pm 0.07) \times 10^{-1}$	$(9.5 \pm 0.4) \times 10^{-2}$
$\langle \mathcal{O}_8^{J/\psi}[^1S_0] \rangle^*$	3.75×10^{-3}	$(0 \pm 1) \times 10^{-4}$	$(2.2 \pm 0.3) \times 10^{-3}$
$\langle \mathcal{O}_8^{\psi(2S)}[^3S_1] \rangle$	4.6×10^{-3}	$(2.5 \pm 0.2) \times 10^{-2}$	$(2.6 \pm 0.2) \times 10^{-2}$
$\langle \mathcal{O}_8^{\psi(2S)}[^1S_0] \rangle^*$	6.5×10^{-4}	$(0 \pm 1) \times 10^{-4}$	$(5 \pm 8) \times 10^{-5}$

Jpsi Data vs. NRQCD: Fit-1

- Fit by p+N Jpsi/psi' data
- Best-fit CO [1S0] and [3S1] LDMEs; CO[1S0]~0

$\langle \mathcal{O}_8^{J/\psi}[^3S_1] \rangle$	6.6×10^{-3}	$(1.47 \pm 0.07) \times 10^{-1}$	$(9.5 \pm 0.4) \times 10^{-2}$	$q\bar{q}$
$\langle \mathcal{O}_8^{J/\psi}[^1S_0] \rangle^*$	3.75×10^{-3}	$(0 \pm 1) \times 10^{-4}$	$(2.2 \pm 0.3) \times 10^{-3}$	
$\langle \mathcal{O}_8^{\psi(2S)}[^3S_1] \rangle$	4.6×10^{-3}	$(2.5 \pm 0.2) \times 10^{-2}$	$(2.6 \pm 0.2) \times 10^{-2}$	$q\bar{q}$
$\langle \mathcal{O}_8^{\psi(2S)}[^1S_0] \rangle^*$	6.5×10^{-4}	$(0 \pm 1) \times 10^{-4}$	$(5 \pm 8) \times 10^{-5}$	

35

Jpsi Data vs. NRQCD: Fit-2

- Fit by p+N Jpsi/psi' and π^-+N Jpsi/psi' data
- Best-fit CO [1S0] and [3S1] LDMEs

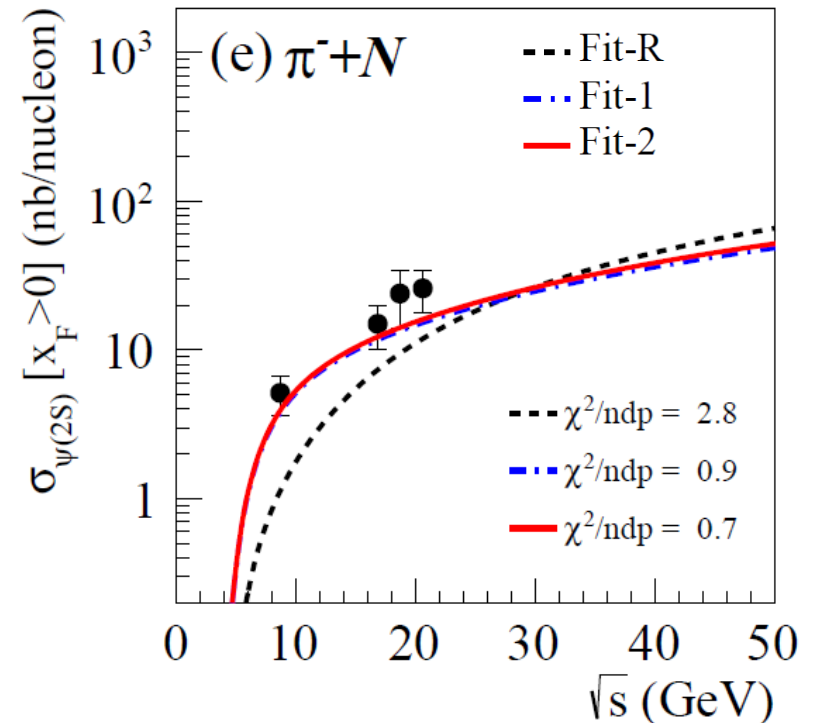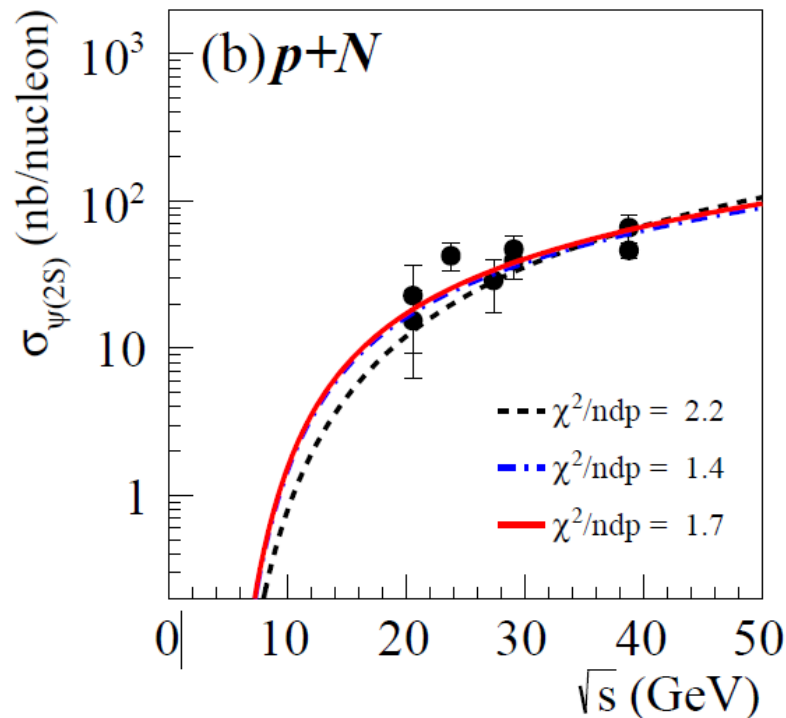|			
$\langle \mathcal{O}_8^{J/\psi}[^3S_1] \rangle$	6.6×10^{-3}	$(1.47 \pm 0.07) \times 10^{-1}$	$(9.5 \pm 0.4) \times 10^{-2}$
$\langle \mathcal{O}_8^{J/\psi}[^1S_0] \rangle^*$	3.75×10^{-3}	$(0 \pm 1) \times 10^{-4}$	$(2.2 \pm 0.3) \times 10^{-3}$
$\langle \mathcal{O}_8^{\psi(2S)}[^3S_1] \rangle$	4.6×10^{-3}	$(2.5 \pm 0.2) \times 10^{-2}$	$(2.6 \pm 0.2) \times 10^{-2}$
$\langle \mathcal{O}_8^{\psi(2S)}[^1S_0] \rangle^*$	6.5×10^{-4}	$(0 \pm 1) \times 10^{-4}$	$(5 \pm 8) \times 10^{-5}$

psi' Data vs. NRQCD

Optimization of CO LDMEs

|	Fit-R	Fit-1	Fit-2
χ^2_{total}/ndf	16.8	6.0	3.3
$\chi^2/ndp|^p_{\sigma(J/\psi)}$	9.2	4.1	5.4
$\chi^2/ndp|^p_{\sigma(\psi(2S))}$	2.2	1.4	1.7
$\chi^2/ndp|^p_{R(\psi(2S))}$	1.1	0.7	1.0
$\chi^2/ndp|^{\pi^-}_{\sigma(J/\psi)}$	46.8	15.3	3.7
$\chi^2/ndp|^{\pi^-}_{\sigma(\psi(2S))}$	2.8	0.9	0.7
$\langle \mathcal{O}_8^{J/\psi}[^3S_1] \rangle$	6.6×10^{-3}	$(1.47 \pm 0.07) \times 10^{-1}$	$(9.5 \pm 0.4) \times 10^{-2}$
$\langle \mathcal{O}_8^{J/\psi}[^1S_0] \rangle^*$	3.75×10^{-3}	$(0 \pm 1) \times 10^{-4}$	$(2.2 \pm 0.3) \times 10^{-3}$
$\langle \mathcal{O}_8^{\psi(2S)}[^3S_1] \rangle$	4.6×10^{-3}	$(2.5 \pm 0.2) \times 10^{-2}$	$(2.6 \pm 0.2) \times 10^{-2}$
$\langle \mathcal{O}_8^{\psi(2S)}[^1S_0] \rangle^*$	6.5×10^{-4}	$(0 \pm 1) \times 10^{-4}$	$(5 \pm 8) \times 10^{-5}$

The description of pion-induced Jpsi and psi' data is significantly improved in Fit-2.

Sensitivity of Data to the Pion PDFs

|	SMRS	GRV	JAM	xFitter
χ^2_{total}/ndf	3.1	3.4	4.8	4.3
$\chi^2/ndp\|^{\pi^-}_{\sigma(J/\psi)}$	2.7	3.7	8.4	6.4
$\chi^2/ndp\|^{\pi^-}_{\sigma(\psi(2S))}$	0.4	0.7	0.4	0.2
$\langle\mathcal{O}_8^{J/\psi}[^3S_1]\rangle$	$(6.9\pm0.3)\times10^{-2}$	$(9.5\pm0.4)\times10^{-2}$	$(8.3\pm0.3)\times10^{-2}$	$(7.4\pm0.9)\times10^{-2}$
$\langle\mathcal{O}_8^{J/\psi}[^1S_0]\rangle^*$	$(3.2\pm0.3)\times10^{-3}$	$(2.2\pm0.3)\times10^{-3}$	$(2.5\pm0.3)\times10^{-3}$	$(2.8\pm0.3)\times10^{-3}$
$\langle\mathcal{O}_8^{\psi(2S)}[^3S_1]\rangle$	$(2.1\pm0.4)\times10^{-2}$	$(2.6\pm0.2)\times10^{-2}$	$(2.6\pm0.1)\times10^{-2}$	$(2.3\pm0.4)\times10^{-2}$
$\langle\mathcal{O}_8^{\psi(2S)}[^1S_0]\rangle^*$	$(2.1\pm1.2)\times10^{-4}$	$(5.0\pm7.9)\times10^{-5}$	$(4.6\pm4.3)\times10^{-5}$	$(1.2\pm7.5)\times10^{-4}$

- The dependence of best-fit LDMEs to the pion PDFs is mild.
- The deficiency of JAM and xFitter in the GG contributions generates a relatively large χ^2 in the description of data.

Subprocesses
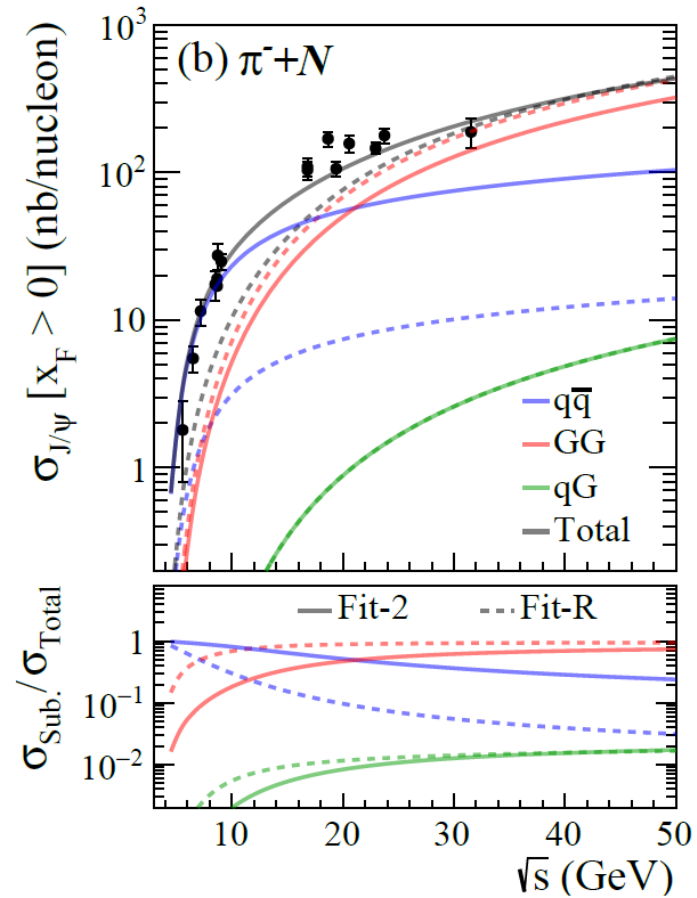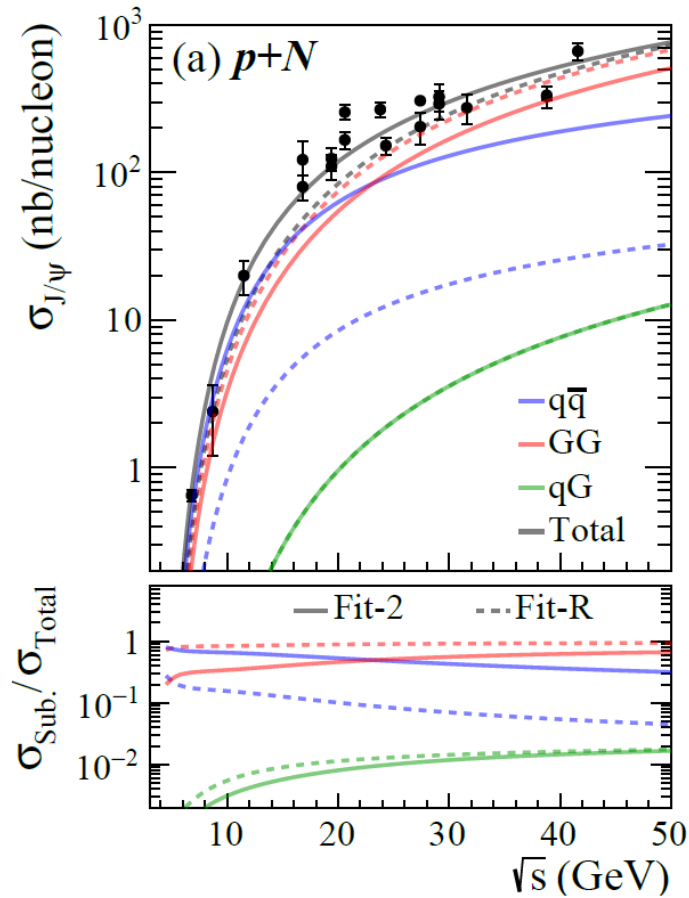
Color States
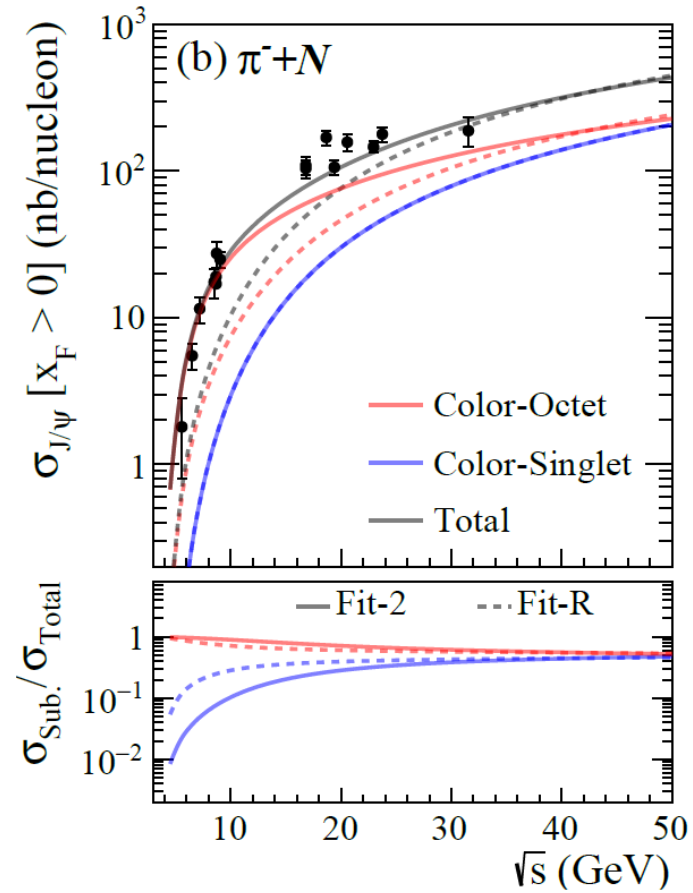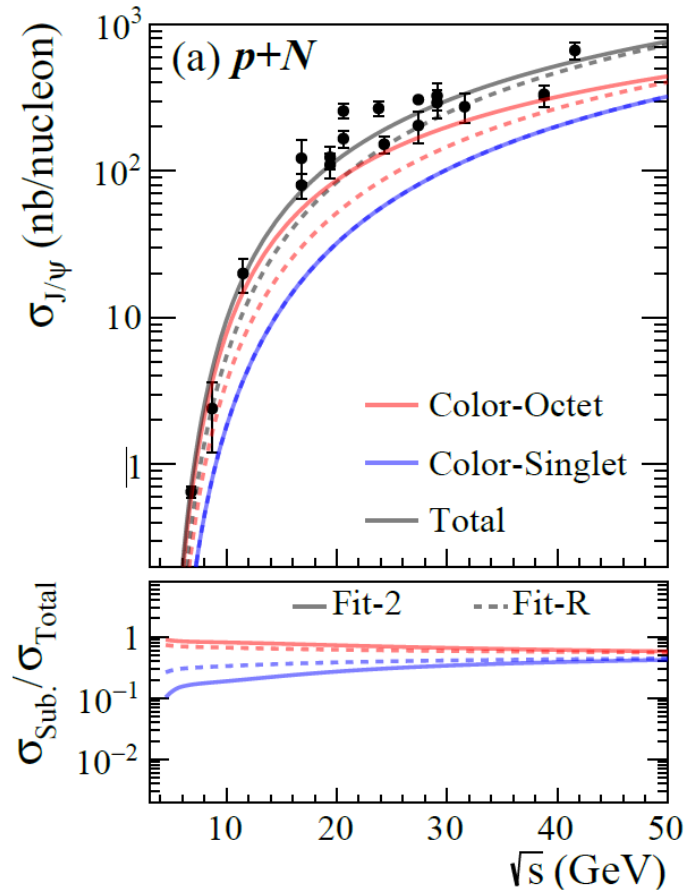
Direct Production and Feeddown